Joint Communication and Trajectory Design for Intelligent Reflecting Surface Empowered UAV SWIPT Networks

Zhendong Li, Wen Chen, *Senior Member, IEEE*, Huanqing Cao, Hongying Tang, Kunlun Wang, *Member, IEEE*, and Jun Li, *Senior Member, IEEE*

***Abstract*—Aiming at the limited battery capacity of widely deployed low-power smart devices in the Internet-of-things (IoT), this paper proposes a novel intelligent reflecting surface (IRS) empowered unmanned aerial vehicle (UAV) simultaneous wireless information and power transfer (SWIPT) network framework, in which IRS is used to reconstruct the wireless channel to enhance the wireless energy transmission efficiency and coverage area of the UAV SWIPT networks. In this paper, we formulate an achievable sum-rate maximization problem by jointly optimizing UAV trajectory, successive interference cancellation (SIC) decoding order, UAV transmit power allocation, power splitting (PS) ratio and IRS reflection coefficient while taking account of user non-orthogonal multiple access (NOMA) and a non-linear energy harvesting model. Due to the coupling of optimization variables, this problem is a complex non-convex optimization problem, and it is challenging to solve it directly. We first transform the problem, and then apply the alternating optimization (AO) algorithm framework to divide the transformed problem into four sub-problems to solve it. Specifically, by applying successive convex approximation (SCA), penalty function method and difference-convex (DC) programming, UAV trajectory, SIC decoding order, UAV transmit power allocation, PS ratio and IRS reflection coefficient are alternately optimized until the convergence is achieved. Numerical simulation results verify the effectiveness of our proposed algorithm compared to other algorithms.**

***Index Terms*—IRS, UAV, simultaneous wireless information and power transfer, NOMA, alternating optimization.**

Manuscript received 21 March 2022; revised 31 May 2022; accepted 31 July 2022. Date of publication 3 August 2022; date of current version 19 December 2022. This work was supported in part by National Key Project under Grants 2020YFB1807700 and 2018YFB1801102, in part by Shanghai Kewei under Grants 20JC1416502 and 22JC1404000, and in part by NSFC under Grant 62071296. The review of this article was coordinated by Dr. Sudip Misra. *(Corresponding author: Wen Chen.)*

Zhendong Li, Wen Chen, and Huanqing Cao are with the Department of Electronic Engineering, Shanghai Jiao Tong University, Shanghai 200240, China (e-mail: lizhendong@sjtu.edu.cn; wenchen@sjtu.edu.cn; caohuanqing@sjtu.edu.cn).

Hongying Tang is with the Science and Technology on Microsystem Laboratory, Shanghai Institute of Microsystem and Information Technology, Chinese Academy of Sciences, Shanghai 200050, China (e-mail: tanghy@mail.sim.ac.cn).

Kunlun Wang is with the School of Communication and Electronic Engineering, East China Normal University, Shanghai 200241, China (e-mail: klwang@cee.ecnu.edu.cn).

Jun Li is with the School of Electronic and Optical Engineering, Nanjing University of Science Technology, Nanjing 210094, China (e-mail: jun.li@njust.edu.cn).

Digital Object Identifier 10.1109/TVT.2022.3196039

I. Introduction

NOWADAYS, with the vigorous development of the Internet-of-things (IoT), the number of smart devices is growing rapidly [1]–[3]. These smart devices for sending and collecting information have the characteristics of low power consumption and limited battery capacity. It is an effective way to replace the battery or charge the battery. However, if the smart devices in IoT are large-scale, such operations are time-consuming and labor-intensive, i.e., its deployment cost increases a lot.

Wireless power transfer (WPT) is a promising technology that can solve the above-mentioned challenges. The technology is flexible, easy to deploy, and does not require contact, so it has received extensive attention from industry and academia [4]–[6]. For devices with low power consumption and limited battery capacity in IoT, wireless charging devices can dynamically join or leave the network, which is more effective. Simultaneous wireless information and power transfer (SWIPT) technology is a scheme in WPT [7]. Through SWIPT, users can get information and energy transmission at the same time, which brings great convenience to the deployment of IoT devices. As one of the design schemes of SWIPT practical receivers, the power splitting (PS) scheme divides the signal received by the receiver into two different power streams, one part is used to decode information, and the other part is used to harvest energy. However, smart devices are usually widely distributed to collect various types of data in IoT, and traditional WPT is not efficient. Therefore, it is challenging for these smart devices to obtain energy from stationary energy stations. Although this problem can be solved by increasing the number of power stations in the target area, this will greatly increase the deployment cost of the network.

In recent years, unmanned aerial vehicles (UAVs) have been widely used in different fields. Compared with traditional fixed access points (APs), UAVs equipped with APs have the advantages of dynamic mobility, flexibility, ease of deployment and low cost [8]–[13]. UAVs equipped with wireless energy stations can better solve the battery capacity limitation problem for widely deployed smart devices in IoT networks. Therefore, the research on UAV-enabled WPT networks has also attracted the attention of the academia [14]–[16]. Sun et al. investigated physical layer security enhancement methods for millimeter-wave (mmWave) UAV SWIPT networks [14].

Wang et al. proposed UAV-assisted non-orthogonal multiple access (NOMA) to achieve SWIPT and guarantee the secure transmission for ground passive receivers (PRs), in which the nonlinear energy harvesting model is applied [15]. However, for UAV-assisted WPT networks, due to distance-related propagation loss, the energy transmission efficiency will decrease as the distance increases, which greatly limits the coverage of UAV-assisted SWIPT. If the wireless channel can be reconstructed and the channel gain can be increased, the coverage area of the networks can be greatly improved, which greatly stimulates the utilization of new networking paradigms to improve the performance for UAV enabled WPT networks.

Intelligent reflecting surface (IRS), also called reconfigurable intelligent surface (RIS), as a revolutionary technology, has been studied extensively by industry and academia [17]–[22], which can reconstruct the wireless channel from the transmitter to the receiver by adjusting the amplitude and phase of the incident signal, thereby improving network performance. In detail, an IRS is an array composed of a large number of low-cost passive reflecting elements, which can be easily deployed on indoor walls or buildings. Since the IRS is a passive device, it only passively reflects the incident signal without signal processing, so it will not introduce unnecessary noise compared with the relay technology [23]. Meanwhile, compared with MIMO technology, since it is not equipped with a complex signal processing unit and it is passive, the required hardware cost and power consumption are much lower [24]. These have greatly promoted the application of IRS in the next generation communication networks.

Based on the advantages of the IRS, the coverage and wireless energy transmission efficiency of the IRS-enabled UAV SWIPT network can be improved. Currently, the optimization and design on the IRS-assisted WPT network [25], [26], the IRS-assisted UAV network [27]–[29], and the UAV WPT network [14]–[16] are in progress. However, the coverage and transmission efficiency potential of these networks cannot be fully released. IRS empowered UAV SWIPT network can well address the above-mentioned challenges in the deployment of IoT devices with limited battery capacity, which is of practical significance. To the best of our knowledge, research on IRS-assisted dynamic UAV WPT networks in IoT scenarios is still in its infancy, which is novel and practical. To fully unleash the potential of drones, we consider the IRS-assisted dynamic UAV SWIPT network while considering user NOMA. In this paper, the achievable sum-rate is maximized by jointly optimizing UAV trajectory, successive interference cancellation (SIC) decoding order, UAV transmit power allocation, PS ratio and IRS reflection coefficient. Due to the high coupling of optimization variables, the concavity and convexity of the objective function and some constraints cannot be determined, so it is challenging to solve this problem directly. Therefore, we need to design an effective algorithm for IRS-assisted UAV-enabled SWIPT networks.

Based on the above background, the main contributions of this paper can be summarized as follows:

- Facing the limited battery capacity of smart devices with widely deployed and low power consumption in IoT networks, we proposed an IRS empowered UAV SWIPT framework. Smart devices apply PS scheme, which allows them to harvest energy while receiving information. In addition, these devices use the NOMA scheme. Meanwhile, we formulate an achievable sum-rate maximization problem by jointly optimizing UAV trajectory, SIC decoding order, UAV transmit power allocation, PS ratio and IRS reflection coefficient. Since this problem is a complicated non-convex optimization problem, it is challenging to solve it directly.
- In order to solve the above sum-rate maximization problem, we first transform the problem, and then use the alternating optimization (AO) framework to divide the transformed problem into four sub-problems. Specifically, first, given UAV transmit power allocation, PS ratio, and IRS reflection coefficient, UAV trajectory and SIC decoding order can be jointly obtained by applying successive convex approximation (SCA) and penalty function method. Given the UAV trajectory, SIC decoding order, UAV transmit power allocation and IRS reflection coefficient, the PS ratio scheme can be obtained. Similarly, UAV transmit power allocation and IRS phase shift coefficients can also be obtained separately by using SCA, penalty function method and difference-convex (DC) programming when the other three variables are given. Finally, the four sub-problems are alternately optimized until convergence is achieved.
- Through numerical simulation, we verify the effectiveness of the proposed optimization algorithm for UAV trajectory, SIC decoding order, UAV transmit power allocation, PS ratio and IRS reflection coefficient compared with the algorithms, i.e., it can improve the achievable sum-rate of the system. For the UAV SWIPT network assisted by IRS, the sum-rate is significantly higher than that of the network without IRS assistance. Meanwhile, as the number of reflecting elements of the IRS increases, the achievable sum-rate can improve.

The remainder of this paper is organized as follows. Section II elaborates the system model and optimization problem formulation for the IRS empowered UAV SWIPT networks. Section III presents the proposed optimization algorithm for the formulated optimization problem. In Section IV, numerical results demonstrate that our algorithm has good convergence and effectiveness. Finally, conclusions are given in Section V.

Notations: Scalars are denoted by lower-case letters, while vectors and matrices are represented by bold lower-case letters and bold upper-case letters, respectively. $|x|$ denotes the absolute value of a complex-valued scalar x, and $\|\mathbf{x}\|$ denotes the Euclidean norm of a complex-valued vector $\mathbf{x}$. $diag(\mathbf{x})$ denotes a diagonal matrix whose diagonal elements are the corresponding elements in vector $\mathbf{x}$. For a square matrix $\mathbf{X}$, $\mathrm{tr}(\mathbf{X})$, $\mathrm{rank}(\mathbf{X})$, $\mathbf{X}^H$ and $\mathbf{X}_{m,n}$ denote its trace, rank, conjugate transpose and m,n-th entry, respectively, while $\mathbf{X} \succeq 0$ represents that $\mathbf{X}$ is a positive semidefinite matrix. $\mathbb{C}^{M\times N}$ denotes the space of $M \times N$ complex matrices. j denotes the imaginary unit, i.e., $j^2 = -1$. $\mathbb{E}\{\cdot\}$ represents the expectation of random variables. Finally, the distribution of a circularly symmetric complex Gaussian (CSCG) random vector with mean μ and covariance matrix $\mathbf{C}$ is denoted by $\mathcal{CN}(\mu, \mathbf{C})$, and $\sim$ stands for 'distributed as'.

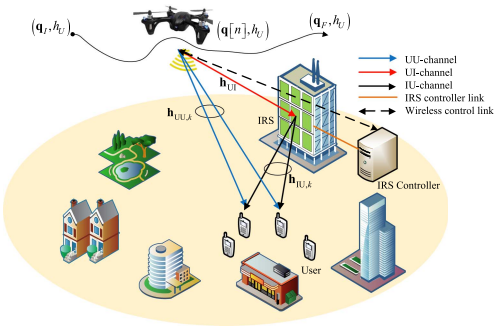

Fig. 1. IRS empowered UAV SWIPT networks.

II. System Model and Problem Formulation

A. System Model

In this paper, we consider an IRS empowered downlink UAV SWIPT network in IoT consisting of a rotary-wing UAV with a single omni-directional antenna, an IRS and K single antenna users (i.e., smart devices with limited battery capacity). As shown as in Fig. 1, the UAV simultaneously sends signals to users. The IRS can be deployed on a building to assist the SWIPT networks from the UAV to users, which is equipped with a uniform linear array (ULA) of M reflecting elements.[1] Meanwhile, the IRS is also equipped with a smart controller, which coordinates the UAV and IRS for both channel acquisition and information and power transmission. We assume that all channels in this paper are quasi-static flat-fading and the channel state information (CSI) of all channels is perfectly known at the UAV. For the channel estimation of IRS empowered UAV networks, we can use state-of-the-art algorithms such as direct cascaded channel estimation [30] and separable cascaded channel estimation [31].

Without loss of generality, we consider a 3D Cartesian coordinate system, where the k-th single-antenna user's coordinate is $\mathbf{w}_k = [x_k, y_k, 0]^T$. The UAV flies at a fixed altitude h_u, which is the minimum altitude to avoid any collision with building. We consider a finite time period T to guarantee the efficiency of simultaneous information and power transmission. For simplicity, the time period T is divided into N time slots, indexed by $n = 1, \ldots, N$. Each time slot $\delta = \frac{T}{N}$ is selected to be small enough to ensure that the UAV position is approximately unchanged when flying at the maximum speed $V_{\max}$. Hence, the 3D trajectory of UAV can be approximated by $\mathbf{q}[n] = [x[n], y[n], h_u]^T, n = 1, \ldots, N$. We consider the initial and final position of the UAV can be denoted by $\mathbf{q}_I$ and $\mathbf{q}_F$, respectively. The trajectory of UAV should satisfy the following constraints

$$\mathbf{q}_I = \mathbf{q}[1], \tag{1}$$

$$\mathbf{q}_F = \mathbf{q}[N], \tag{2}$$

$$\|\mathbf{q}[n+1] - \mathbf{q}[n]\|^2 \le (V_{\max}\delta)^2, n = 1, \ldots, N-1. \tag{3}$$

[1]It is worth noting that the algorithm proposed in this paper can be extended to the IRS equipped with a uniform planar array (UPA) by considering the corresponding antenna array response.

For the IRS with M reflecting elements, each element reflects the received signal from the UAV with an adjustable amplitude and phase shift. Let $\boldsymbol{\theta}[n] = [\theta_1[n], \ldots, \theta_M[n]]^T \in \mathbb{C}^{M\times 1}, \forall n$, and we model the IRS reflection matrix by using $\boldsymbol{\Theta}[n] = diag(\beta_1[n]e^{j\theta_1[n]}, \ldots, \beta_M[n]e^{j\theta_M[n]}) \in \mathbb{C}^{M\times M}$, where $\theta_m[n] \in [0, 2\pi), \forall m, n$ and $\beta_m[n] \in [0, 1], \forall m, n$ denote the phase shift and amplitude reflection coefficient of the m-th IRS element, respectively. For simplicity, we set $\beta_m[n] = 1$ to achieve the maximum reflecting power gain. In the n-th time slot, the phase shift of the m-th element should satisfy the following constraint

$$0 \le \theta_m[n] < 2\pi, \forall m, n. \tag{4}$$

Furthermore, the first element of the IRS is regarded as the reference point whose 3D coordinate can be denoted by $\mathbf{w}_r = [x_r, y_r, h_r]^T$, respectively. Hence, the distance between the IRS and the UAV or the ground users can be approximated by that between the reference point and the corresponding node. The channel gain from the UAV to the IRS, from the UAV to the k-th ground user, and from the IRS to the k-th ground user can be denoted by $\mathbf{h}_{\mathrm{UI}} \in \mathbb{C}^{M\times 1}$, $h_{\mathrm{UU},k} \in \mathbb{C}$, and $\mathbf{h}_{\mathrm{IU},k} \in \mathbb{C}^{M\times 1}$, respectively.

Since the UAV usually flies at a high altitude and the IRS is commonly placed on the building, the channel from the UAV to the IRS (i.e., UI-channel) can be modeled to be a line-of-sight (LoS) channel. Since the UAV is flying or hovering at a certain height in the air, the channel from the UAV to the k-th user (i.e., UU-channel) has both LoS and non-line-of-sight (NLoS) components, so we model it as a Rician channel [32]. Besides, the channel from the IRS to the k-th ground user (i.e., IU-channel) can also be modeled by a Rician fading channel. The LoS component of the channel associated with the IRS can be expressed by the responses of the ULA. The array response of M-element ULA of the IRS in the n-th time slot can be given by

$$\mathbf{h}[n] = \left[1, e^{-j2\pi\frac{d}{\lambda}\cos\phi[n]}, \ldots, e^{-j2\pi\frac{d}{\lambda}(M-1)\cos\phi[n]}\right]^T, \forall n, \tag{5}$$

where $\phi[n]$ is angle-of-arrival (AoA) from the UAV to the IRS in the n-th time slot, $\cos\phi[n] = \frac{x_r - x[n]}{d_{\mathrm{UI}}[n]}$ with $d_{\mathrm{UI}}[n] = \|\mathbf{q}[n] - \mathbf{w}_r\|$ denotes the distance from the UAV to the IRS in the n-th time slot, λ is the carrier wavelength, and d represents the array interval. Therefore, the channel gain of the UI-channel in the n-th time slot can be denoted by

$$\mathbf{h}_{\mathrm{UI}}[n] = \sqrt{\frac{\beta_0}{(d_{\mathrm{UI}}[n])^2}}\mathbf{h}[n], \forall n, \tag{6}$$

where β_0 is the path loss when the reference distance is 1 m. In addition, the channel gain of the UU-channel in the n-th time slot can be expressed by

$$h_{\mathrm{UU},k}[n] = \sqrt{\frac{\beta_0}{(d_{\mathrm{UU},k}[n])^\alpha}}\left(\sqrt{\frac{\kappa_1}{1+\kappa_1}}h_{\mathrm{UU},k}^{\mathrm{LoS}}[n] + \sqrt{\frac{1}{1+\kappa_1}}h_{\mathrm{UU},k}^{\mathrm{NLoS}}[n]\right), \forall k, n, \tag{7}$$

where α is the corresponding path loss exponent related to the UU-channel and κ_1 is the Rician factor.[2] $d_{\mathrm{UU},k}[n] = \|\mathbf{q}[n] - \mathbf{w}_k\|$ denotes the distance from the UAV to the k-th user in the n-th time slot. $h^{\mathrm{LoS}}_{\mathrm{UU},k}[n] = 1$ and $h^{\mathrm{NLoS}}_{\mathrm{UU},k}[n] \sim \mathcal{CN}(0,1)$ represents the random scattering component. Similarly, the channel gain of the IU-channel can be denoted by

$$\mathbf{h}_{\mathrm{IU},k} = \sqrt{\frac{\beta_0}{(d_{\mathrm{IU},k})^{\gamma}}}\left(\sqrt{\frac{\kappa_2}{1+\kappa_2}}\mathbf{h}^{\mathrm{LoS}}_{\mathrm{IU},k} + \sqrt{\frac{1}{1+\kappa_2}}\mathbf{h}^{\mathrm{NLoS}}_{\mathrm{IU},k}\right), \forall k, \tag{8}$$

where γ is the corresponding path loss exponent related to the IU-channel, and κ_2 is the Rician factor. $d_{\mathrm{IU},k} = \|\mathbf{w}_r - \mathbf{w}_k\|$ denotes the distance from the IRS to the k-th user in the n-th time slot. The LoS component $\mathbf{h}^{\mathrm{LoS}}_{\mathrm{IU},k} \in \mathbb{C}^{M\times 1}$ can be denoted by

$$\mathbf{h}^{\mathrm{LoS}}_{\mathrm{IU},k} = \left[1, e^{j2\pi\frac{d}{\lambda}\cos\varphi_k}, \ldots, e^{j2\pi\frac{d}{\lambda}(M-1)\cos\varphi_k}\right]^T, \forall k, \tag{9}$$

where φ_k is the angle-of-departure (AoD) from the IRS to the k-th user, $\cos\varphi_k = \frac{x_k - x_r}{d_{\mathrm{IU},k}}$. The NLoS component can be denoted by $\mathbf{h}^{\mathrm{NLoS}}_{\mathrm{IU},k} \sim \mathcal{CN}(\mathbf{0}, \mathbf{I}_M)$. Therefore, with the aid of the IRS, the combined channel power gain from the UAV to the k-th user in the n-th time slot can be expressed as

$$H_k[n] = \left|h_{\mathrm{UU},k}[n] + \mathbf{h}^H_{\mathrm{IU},k}\boldsymbol{\Theta}[n]\,\mathbf{h}_{\mathrm{UI}}[n]\right|^2, \forall k, n. \tag{10}$$

In this paper, we assume that all uses share the same frequency, thus the UAV applies NOMA to provide communication for the users. specifically, the transmission signal of UAV by invoking superposition coding (SC) can be denoted as $\tilde{s} = \sum_{k=1}^{K}\sqrt{p_k[n]}s_k[n]$, where $s_k[n] \sim \mathcal{CN}(0,1)$ denotes the transmission data sent by UAV to the k-th user, and $p_k[n]$ denotes the transmit power allocated to the k-th user in the n-th time slot. Without loss of generality, it should satisfy the following constraints

$$p_k[n] \geq 0, \forall k, n, \tag{11}$$

$$\sum_{k=1}^{K} p_k[n] \leq P_{\max}, \forall n, \tag{12}$$

where $P_{\max}$ denotes the maximum transmit power of the UAV.

Therefore, the signal received by the k-th user in the n-th slot can be expressed as

$$\begin{aligned} y_k[n] = &\underbrace{\left(h_{\mathrm{UU},k}[n] + \mathbf{h}^H_{\mathrm{IU},k}\boldsymbol{\Theta}[n]\,\mathbf{h}_{\mathrm{UI}}[n]\right)\sqrt{p_k[n]}s_k[n]}_{\text{desired signal}} \\ &+ \underbrace{\left(h_{\mathrm{UU},k}[n] + \mathbf{h}^H_{\mathrm{IU},k}\boldsymbol{\Theta}[n]\,\mathbf{h}_{\mathrm{UI}}[n]\right)\sum_{i\neq k}^{K}\sqrt{p_i[n]}s_i[n]}_{\text{interference signal}} \\ &+ n_k, \forall k, n, \end{aligned} \tag{13}$$

where $n_k \sim \mathcal{CN}(0, \sigma_k^2)$ is additive white Gaussian noise (AWGN).

[2]In fact, the Rician factor is related to the trajectory of the UAV [33]. Since the channel gain between the UAV and the user is largely dependent on the path loss caused by the distance, for the convenience of analysis, we assume that the Rician factor in each time slot is fixed.

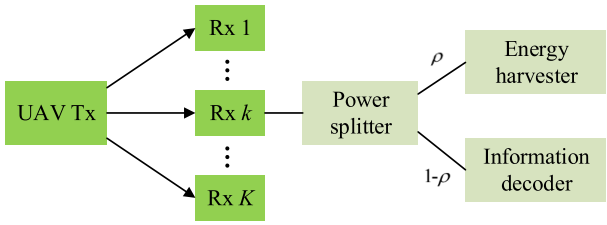

Fig. 2. PS receiver architecture.

According to the NOMA mechanism, each user adopts SIC to remove inter-user interference. Specifically, a user with a stronger channel power gain first decodes the signal of a user with a weaker power channel gain before decoding its own signal. Therefore, the decoding order needs to be paid more attention in NOMA. Herein, we introduce a set of binary variables $\psi_{i,k}[n] \in \{0,1\}, \forall n, i \neq k$ to describe the decoding order among users. If the channel power gain of the i-th user is stronger than that of the k-th user in the n-th time slot, we let $\psi_{i,k}[n] = 1$. Otherwise, $\psi_{i,k}[n] = 0$. Therefore, it should satisfy the following constraints:

$$\psi_{i,k}[n] = \begin{cases} 1, & \text{if } H_i[n] > H_k[n] \\ 0, & \text{otherwise} \end{cases}, \tag{14}$$

$$\psi_{i,k}[n] + \psi_{k,i}[n] = 1, \forall n, i \neq k. \tag{15}$$

Moreover, for a given decoding order, the UAV transmit power allocation should satisfy

$$p_k[n] \geq \psi_{i.k}p_i[n], \forall n, i \neq k, \tag{16}$$

which ensures that higher power needs to be allocated to users with weaker channel power gain [34]. This communication method can well guarantee the fairness of users, i.e., it can well guarantee the communication of users with weaker channel conditions.

In addition, we consider the power splitting (PS) receiver architecture at the users for information decoding and energy harvesting, which is actually one of the most widely used architectures in SWIPT networks. The architecture diagram is shown in the Fig. 2. Specifically, In the n-th time slot, the radio frequency (RF) signal received by the k-th ground user is split with a PS ratio $\rho_k[n]$, which should satisfy the following constraint

$$0 \leq \rho_k[n] \leq 1, \forall k, n, \tag{17}$$

which represents the PS ratio of each ground user in the n-th time slot should be between zero and one. The $\rho_k[n]$ portion of the received power is used by the k-th user for energy harvesting in the n-th time slot, and the remaining $(1-\rho_k[n])$ portion is used by the k-th user for decoding information in the n-th time slot. Hence, the signal split to the k-th user in the n-th time slot for decoding information can be denoted by

$$\begin{aligned} y^{\mathrm{ID}}_k[n] = \sqrt{1-\rho_k[n]}\Big(&\left(h_{\mathrm{UU},k}[n] + \mathbf{h}^H_{\mathrm{IU},k}\boldsymbol{\Theta}[n]\,\mathbf{h}_{\mathrm{UI}}[n]\right) \\ &\sum_{i=1}^{K}\sqrt{p_i[n]}s_i[n] + n_k\Big) + z_k, \forall k, n, \end{aligned} \tag{18}$$

where $z_k \sim \mathcal{CN}(0, \delta_k^2)$ denotes the noise introduced by information decoder for the k-th user.

Therefore, the received signal to interference plus noise ratio (SINR) of the k-th user by applying SIC for information decoding in the n-th slot can be expressed as

$$\mathrm{SINR}_k[n] = \frac{(1-\rho_k[n])\, p_k[n]\, H_k[n]}{(1-\rho_k[n])\left(\sum_{i\neq k}^{K} \psi_{i,k}[n]\, p_i[n]\, H_k[n] + \sigma_k^2\right) + \delta_k^2}, \quad \forall n, i \neq k, \tag{19}$$

Therefore, the achievable rate (bps/Hz) of the k-th user in the n-th time slot can be expressed as

$$R_k[n] = \log_2\left(1 + \mathrm{SINR}_k[n]\right), \forall k, n. \tag{20}$$

The achievable sum-rate in the time period T can be expressed as

$$R_{\mathrm{sum}} = \sum_{n=1}^{N}\sum_{k=1}^{K} R_k[n]. \tag{21}$$

In addition, the signal split to the k-th user in the n-th time slot for harvesting energy can be denoted by

$$y_k^{\mathrm{EH}}[n] = \sqrt{\rho_k[n]}\left(\left(h_{\mathrm{UU},k}[n] + \mathbf{h}_{\mathrm{IU},k}^H \boldsymbol{\Theta}[n]\, \mathbf{h}_{\mathrm{UI}}[n]\right) \sum_{i=1}^{K}\sqrt{p_i[n]}s_i[n] + n_k\right), \forall k, n. \tag{22}$$

Hence, the received power of the k-th user in the n-th time slot can be given by

$$P_k[n] = \rho_k[n]\left(\sum_{i=1}^{K} p_i[n]\, H_k[n] + \sigma_k^2\right), \forall k, n. \tag{23}$$

Furthermore, in order to accurately describe the energy harvesting, this paper adopts the non-linear energy harvesting model based on the practical system, thus the harvesting power of the k-th user in the n-th time can be given by

$$\Xi(P_k[n]) = \left(\frac{\xi_k}{X_k\left(1+\exp\left(-a_k\left(P_k[n]-b_k\right)\right)\right)} - Y_k\right), \forall k, n, \tag{24}$$

where ξ_k denotes the maximum power that the k-th user can harvest, a_k and b_k are parameters related to specific circuit specifications, $X_k = \exp(a_k b_k)(1+\exp(a_k b_k))$ and $Y_k = \xi_k \exp(a_k b_k)$ [35]. Then the energy harvesting of the k-th user in the n-th time slot can be expressed as

$$E_k[n] = \delta\Xi\left(P_k[n]\right), \forall k, n, \tag{25}$$

In order to meet the energy constraint of the k-th user in the n-th time slot, $E_k[n]$ needs to meet the following constraint

$$E_k[n] \geq \chi_{th}, \forall k, n, \tag{26}$$

where χ_{th} is the energy threshold of the k-th user in the n-th time slot. It can be seen from (20) and (26) that there is a tradeoff between the achievable rate and energy harvesting for the k-th user in the n-th time slot.

B. Problem Formulation

In this paper, we maximize the achievable sum-rate for all users in the IRS empowered UAV SWIPT networks by jointly optimizing UAV trajectory $\mathbf{Q} = \{\mathbf{q}[n], \forall n\}$, SIC decoding order $\boldsymbol{\psi} = \{\psi_{i,k}[n], \forall n, i \neq k\}$, UAV transmit power allocation $\mathbf{p} = \{p_k[n], \forall k, n\}$, PS ratio $\boldsymbol{\rho} = \{\rho_k[n], \forall k, n\}$ and IRS reflection coefficient $\boldsymbol{\theta} = \{\theta_m[n], \forall m, n\}$. The optimization problem can be formulated as follows

$$\mathcal{P}0: \quad \max_{\mathbf{Q},\mathbf{p},\boldsymbol{\psi},\boldsymbol{\rho},\boldsymbol{\theta}} \; R_{\mathrm{sum}}, \tag{27a}$$

$$\text{s.t.} \quad \mathbf{q}_I = \mathbf{q}[1], \tag{27b}$$

$$\mathbf{q}_F = \mathbf{q}[N], \tag{27c}$$

$$\|\mathbf{q}[n+1] - \mathbf{q}[n]\|^2 \leq (V_{\max}\delta)^2, n = 1, \ldots, N-1, \tag{27d}$$

$$p_k[n] \geq 0, \forall k, n, \tag{27e}$$

$$\sum_{k=1}^{K} p_k[n] \leq P_{\max}, \forall n, \tag{27f}$$

$$0 \leq \theta_m[n] \leq 2\pi, \forall m, n, \tag{27g}$$

$$0 \leq \rho_k[n] \leq 1, \forall k, n, \tag{27h}$$

$$\psi_{i,k}[n] = \begin{cases} 1, & \text{if } H_i[n] > H_k[n] \\ 0, & \text{otherwise} \end{cases}, \tag{27i}$$

$$\psi_{i,k}[n] + \psi_{k,i}[n] = 1, \forall n, i \neq k, \tag{27j}$$

$$p_k[n] \geq \psi_{i.k} p_i[n], \forall n, i \neq k, \tag{27k}$$

$$E_k[n] \geq \chi_{th}, \forall k, n, \tag{27l}$$

where (27b)-(27 d) denote the UAV trajectory constraint. (27e), (27f) and (27 k) are the UAV transmit power allocation constraint. (27 g) denotes the IRS reflection coefficients constraint and (27 h) is the PS ratio constraint in SWIPT. (27i) and (27j) are the SIC decoding order constraint in NOMA. (27 l) denotes the energy harvesting threshold constraint. It can be seen that the joint optimizaton problem $\mathcal{P}0$ is a non-convex optimization problem since the optimization variables are highly coupled, and the objective function is not joint concave with respect to (w.r.t.) the optimization variables. In addition, the constraints (27i)-(27 k) contain binary constraints. Hence, the problem $\mathcal{P}0$ is a mixed integer non-convex optimization problem, and it is challenging to solve the problem $\mathcal{P}0$ directly. Next, based on the AO algorithm framework, we propose an efficient iterative algorithm to obtain a high-quality suboptimal solution.

III. Joint Optimization Algorithm for the IRS Empowered UAV SWIPT Networks

Since the objective function of problem $\mathcal{P}0$ contains random variables, we take expectation on it to transform the problem. Then, for the transformed problem, we use AO algorithm to solve it. More specifically, we divide the optimization problem into four sub-problmes, i.e., $\{\mathbf{Q}, \boldsymbol{\psi}\}$, $\mathbf{p}$, $\boldsymbol{\rho}$ and $\boldsymbol{\theta}$. For given UAV transmit power allocation $\mathbf{p}$, user PS ratio $\boldsymbol{\rho}$ and IRS reflection coefficient $\boldsymbol{\theta}$, the trajectory of UAV $\mathbf{Q}$ and SIC decoding order $\boldsymbol{\psi}$ can be obtained. Next, for given the UAV trajectory $\mathbf{Q}$, SIC

decoding order $\boldsymbol{\psi}$, UAV transmit power allocation $\mathbf{p}$ and user PS ratio $\boldsymbol{\rho}$, we can get the IRS reflection coefficient $\boldsymbol{\theta}$. Then, UAV transmit power allocation $\mathbf{p}$ can be obtained when the UAV trajectory $\mathbf{Q}$, SIC decoding order $\boldsymbol{\psi}$, IRS reflection coefficient $\boldsymbol{\theta}$ and user PS ratio $\boldsymbol{\rho}$ are fixed. Fianlly, We can also get user PS ratio $\boldsymbol{\rho}$ by fixing the UAV trajectory $\mathbf{Q}$, SIC decoding order $\boldsymbol{\psi}$, IRS reflection coefficient $\boldsymbol{\theta}$ and UAV transmit power allocation $\mathbf{p}$. The four sub-problems are optimized alternately until convergence is achieved, and the SCA, penalty function method and DC programming are applied when we solving the above sub-problems. Herein, we first introduce the joint UAV trajectory, SIC decoding order, UAV transmit power allocation, PS ratio and IRS reflection coefficient optimization algorithm, and then explain in detail how to solve each sub-problem. The overall optimization algorithm can be summarized as Algorithm 1.

A. Optimization Problem Transformation

Since the objective function $R_k[n]$ of the optimization problem $\mathcal{P}0$ contains random variables, we take the expectation $\mathbb{E}\{R_k[n]\}$ to analyze it. Since the probability distribution of $R_k[n]$ is difficult to obtain, it is not easy to find a closed-form solution of $\mathbb{E}\{R_k[n]\}$. Thus, we use the following Lemma 1 to approximate $\mathbb{E}\{R_k[n]\}$.

Lemma 1: If X is a positive independent random variable, for any $\phi > 0$, $\omega > 0$ and $\varphi > 0$, the following approximation result holds

$$\mathbb{E}\left\{\log_2\left(1+\frac{\phi}{\varphi+\frac{\omega}{X}}\right)\right\} \approx \mathbb{E}\left\{\log_2\left(1+\frac{\phi}{\varphi+\frac{\omega}{\mathbb{E}\{X\}}}\right)\right\}. \tag{28}$$

Proof: The proof of Lemma 1 is similar to Theorem 1 in [36], which is omitted here.

We first take an expectation of $H_k[n]$ as shown in (29) at the bottom of this page, with

$$\widehat{h}_{\mathrm{UU},k}[n] = \sqrt{\frac{\vartheta_1}{(d_{\mathrm{UU},k}[n])^{\alpha}}}h_{\mathrm{UU},k}^{\mathrm{LoS}}[n],$$

$$\breve{h}_{\mathrm{UU},k}[n] = \sqrt{\frac{\beta_0-\vartheta_1}{(d_{\mathrm{UU},k}[n])^{\alpha}}}h_{\mathrm{UU},k}^{\mathrm{NLoS}}[n],$$

$$\widehat{\mathbf{h}}_{\mathrm{IU},k} = \sqrt{\frac{\vartheta_2}{(d_{\mathrm{IU},k})^{\gamma}}}\mathbf{h}_{\mathrm{IU},k}^{\mathrm{LoS}},$$

$$\breve{\mathbf{h}}_{\mathrm{IU},k} = \sqrt{\frac{\beta_0-\vartheta_2}{(d_{\mathrm{IU},k})^{\gamma}}}\mathbf{h}_{\mathrm{IU},k}^{\mathrm{NLoS}},$$

$$\vartheta_1 = \frac{\beta_0\kappa_1}{1+\kappa_1} \quad \vartheta_2 = \frac{\beta_0\kappa_2}{1+\kappa_2}.$$

According to Lemma 1, the expectation of the objective function $R_k[n]$ can be approximately expressed as (30), shown at the bottom of this page. Therefore, the objective function of problem $\mathcal{P}0$ can be transformed into $\tilde{R}_{\mathrm{sum}}$, which can be expressed as

$$\tilde{R}_{\mathrm{sum}} = \sum_{n=1}^{N}\sum_{k=1}^{K}\tilde{R}_k[n]. \tag{31}$$

In addition, according to (14), it can be seen that the SIC decoding order of users is determined by $H_k[n]$. For ease of analysis, we approximate (14) as

$$\psi_{i,k}[n] = \begin{cases} 1, & \text{if } d_{\mathrm{UU},k}[n] > d_{\mathrm{UU},i}[n] \\ 0, & \text{otherwise} \end{cases}. \tag{32}$$

This approximation indicates that the decoding order of the users is determined by the distance between the user and the UAV, which has practical significance. First, the cascaded channels of UI-channel and IU-channel have a large path loss, so the channel power gain is largely determined by the UU-channel. Second,

$$\begin{aligned}
\mathbb{E}\{H_k[n]\} &= \mathbb{E}\left\{\left|\left(\widehat{h}_{\mathrm{UU},k}[n]+h_{\mathrm{UU},k}[n]\right)+\left(\widehat{\mathbf{h}}_{\mathrm{IU},k}^H+\breve{\mathbf{h}}_{\mathrm{IU},k}^H\right)\boldsymbol{\Theta}[n]\,\mathbf{h}_{\mathrm{UI}}[n]\right|^2\right\} \\
&= \left|\widehat{h}_{\mathrm{UU},k}[n]+\widehat{\mathbf{h}}_{\mathrm{IU},k}^H\boldsymbol{\Theta}[n]\,\mathbf{h}_{\mathrm{UI}}[n]\right|^2+\mathbb{E}\left\{\left|\breve{h}_{\mathrm{UU},k}[n]\right|^2\right\}+\mathbb{E}\left\{\left|\breve{\mathbf{h}}_{\mathrm{IU},k}^H\boldsymbol{\Theta}[n]\,\mathbf{h}_{\mathrm{UI}}[n]\right|^2\right\} \\
&= \left|\widehat{h}_{\mathrm{UU},k}[n]+\widehat{\mathbf{h}}_{\mathrm{IU},k}^H\boldsymbol{\Theta}[n]\,\mathbf{h}_{\mathrm{UI}}[n]\right|^2+\frac{\beta_0-\vartheta_1}{(d_{\mathrm{UU},k}[n])^{\alpha}}+\frac{M\beta_0(\beta_0-\vartheta_2)}{(d_{\mathrm{UI}}[n])^2(d_{\mathrm{IU},k})^{\gamma}} \\
&\triangleq \xi_k[n], \forall k,n
\end{aligned} \tag{29}$$

$$\begin{aligned}
\mathbb{E}\{R_k[n]\} &\approx \mathbb{E}\left\{\log_2\left(1+\frac{(1-\rho_k[n])\,p_k[n]}{(1-\rho_k[n])\sum_{i\neq k}^{K}\psi_{i,k}[n]\,p_i[n]+\frac{(1-\rho_k[n])\sigma_k^2+\delta_k^2}{\mathbb{E}\{H_k[n]\}}}\right)\right\} \\
&= \log_2\left(1+\frac{(1-\rho_k[n])\,p_k[n]}{(1-\rho_k[n])\sum_{i\neq k}^{K}\psi_{i,k}[n]\,p_i[n]+\frac{(1-\rho_k[n])\sigma_k^2+\delta_k^2}{\xi_k[n]}}\right)\triangleq\tilde{R}_k[n], \forall n, i\neq k
\end{aligned} \tag{30}$$

Algorithm 1: Joint UAV Trajectory, SIC Decoding Order, UAV transmit power Allocation, PS Ratio and IRS Reflection Coefficient Optimization Algorithm.

1: Initialize $\mathbf{Q}^{(0)}$, $\boldsymbol{\psi}^{(0)}$, $\boldsymbol{\rho}^{(0)}$, $\mathbf{p}^{(0)}$ and $\boldsymbol{\theta}^{(0)}$. Let $r=0$, $\varepsilon=10^{-3}$.
2: **repeat**
3: Solve the sub-problem 1 for given $\boldsymbol{\rho}^{(r)}$, $\mathbf{p}^{(r)}$ and $\boldsymbol{\theta}^{(r)}$, and obtain UAV trajectory $\mathbf{Q}^{(r+1)}$ and SIC decoding order $\boldsymbol{\psi}^{(r+1)}$.
4: Solve the sub-problem 2 for given $\mathbf{Q}^{(r)}$, $\boldsymbol{\psi}^{(r)}$, $\mathbf{p}^{(r)}$ and $\boldsymbol{\theta}^{(r)}$, and obtain PS ratio $\boldsymbol{\rho}^{(r+1)}$.
5: Solve the sub-problem 3 for given $\mathbf{Q}^{(r)}$, $\boldsymbol{\psi}^{(r)}$, $\boldsymbol{\rho}^{(r)}$ and $\boldsymbol{\theta}^{(r)}$, and obtain UAV transmit power allocation $\mathbf{p}^{(r+1)}$.
6: Solve the sub-problem 4 for given $\mathbf{Q}^{(r)}$, $\boldsymbol{\psi}^{(r)}$, $\boldsymbol{\rho}^{(r)}$ and $\mathbf{p}^{(r)}$, and obtain IRS reflection coefficient $\boldsymbol{\theta}^{(r+1)}$.
7: Update $r=r+1$.
8: **until** The fractional decrease of the objective value is below a threshold ε.
9: **return**UAV trajectory, SIC decoding order, UAV transmit power allocation, PS ratio and IRS reflection coefficient.

for UU-channel, small-scale fading is negligible compared to large-scale fading. Therefore, the channel power gain is usually determined by the distance from the UAV to the user, i.e., the shorter the distance, the higher the channel power gain.

Therefore, the optimization problem $\mathcal{P}0$ can be transformed into the problem $\mathcal{P}1$ as follows

$$\mathcal{P}1: \max_{\mathbf{Q},\mathbf{p},\boldsymbol{\psi},\boldsymbol{\rho},\boldsymbol{\theta}} \tilde{R}_{\mathrm{sum}}, \tag{33a}$$

$$\text{s.t.} \quad \text{(27b)–(27h), (32), (27j)–(27l).} \tag{33b}$$

B. Optimization of UAV Trajectory $\mathbf{Q}$ *and SIC Decoding Order* $\boldsymbol{\psi}$

Given UAV transmit power allocation $\mathbf{p}$, user PS ratio $\boldsymbol{\rho}$ and IRS reflection coefficient $\boldsymbol{\theta}$, the UAV trajectory $\mathbf{Q}$ and SIC decoding order $\boldsymbol{\psi}$ optimization problem can be given by

$$\mathcal{P}2: \max_{\mathbf{Q},\boldsymbol{\psi}} \tilde{R}_{\mathrm{sum}}, \tag{34a}$$

$$\text{s.t.} \quad \text{(27b)–(27d), (27i)–(27l).} \tag{34b}$$

The problem $\mathcal{P}2$ is still a mixed integer non-convex optimization problem due to the non-concave objective function, integer constraints (27i)-(27 k) and non-convex constraint (27 l). Herein, we introduce some auxiliary variables to deal with the problem $\mathcal{P}2$. Let $\{u_k[n]>0,\forall k,n\}$ denote the upper bound of $d_{\mathrm{UU},k}[n]$, and $\{u[n]>0,\forall n\}$ denote the upper bound of $d_{\mathrm{UI}}[n]$. Therefore, they satisfy

$$\left(u_k\left[n\right]\right)^2 \geq \left\|\mathbf{q}\left[n\right]-\mathbf{w}_k\right\|^2, \forall k,n, \tag{35}$$

$$\left(u\left[n\right]\right)^2 \geq \left\|\mathbf{q}\left[n\right]-\mathbf{w}_r\right\|^2, \forall k. \tag{36}$$

Therefore, the lower bound of the expected combined channel power gain, denoted by $\{\underline{\xi}_k[n],\forall k,n\}$, can be expressed as

$$\underline{\xi}_k\left[n\right] = \beta_0\left(u_k\left[n\right]\right)^{-\alpha} + A_k\left[n\right]\left(u\left[n\right]\right)^{-2} + B_k\left[n\right]\left(u_k\left[n\right]\right)^{-\alpha 2}\left(u\left[n\right]\right)^{-1}, \forall k,n, \tag{37}$$

$A_k[n]=\beta_0|\widehat{\mathbf{h}}_{\mathrm{IU},k}^H\boldsymbol{\Theta}[n]\mathbf{h}[n]|^2+M\beta_0(\beta_0-\vartheta_2)(d_{\mathrm{IU},k})^{-\gamma}$ and $B_k[n]=2\mathrm{Re}\{\sqrt{\vartheta_1\beta_0}\widehat{\mathbf{h}}_{\mathrm{IU},k}^H\boldsymbol{\Theta}[n]\mathbf{h}[n]\}$, $\mathrm{Re}\{\cdot\}$ is the operator for taking the real part of complex numbers. In addition, we further introduce the auxiliary variable as follows

$$\Lambda_k\left[n\right]=\left(1-\rho_k\left[n\right]\right)\sum_{i\neq k}^{K}\psi_{i,k}\left[n\right]p_i\left[n\right]+\frac{\left(1-\rho_k\left[n\right]\right)\sigma_k^2+\delta_k^2}{\underline{\xi}_k\left[n\right]}, \tag{38}$$

Accordingly, the objective function of problem $\mathcal{P}2$ can be lower bounded by

$$\tilde{R}_k\left[n\right] \geq \log_2\left(1+\frac{\left(1-\rho_k\left[n\right]\right)p_k\left[n\right]}{\Lambda_k\left[n\right]}\right), \forall n, i\neq k, \tag{39}$$

where the equation holds when (35) and (36) are equal respectively.

In addition, the binary constraint (27i) can be transformed into the following constraints with continuous variables between 0 and 1,

$$\psi_{i,k}\left[n\right]\left(1-\psi_{i,k}\left[n\right]\right)\leq 0, \forall n, i\neq k, \tag{40}$$

$$0\leq\psi_{i,k}\left[n\right]\leq 1, \forall n, i\neq k, \tag{41}$$

$$d_{\mathrm{UU},i}\left[n\right]\leq\pi_i\left[n\right], \forall n, i, \tag{42}$$

$$\psi_{i,k}\left[n\right]\pi_i\left[n\right]\leq d_{\mathrm{UU},k}\left[n\right], \forall n, k\neq i, \tag{43}$$

where (40) and (41) make the continuous variable $\psi_{i,k}[n]$ either 0 or 1. The auxiliary variable $\{\pi_i[n],\forall n,i\}$ represents the upper bound of $d_{\mathrm{UU},i}[n]$, and (42) and (43) ensure that when $d_{\mathrm{UU},i}[n]<d_{\mathrm{UU},k}[n]$, $\psi_{i,k}[n]=1$.

Therefore, the problem $\mathcal{P}2$ can be equivalently transformed into

$$\mathcal{P}2.1: \max_{\mathbf{Q},\boldsymbol{\psi},\Upsilon}\sum_{n=1}^{N}\sum_{k=1}^{K}\log_2\left(1+\frac{\left(1-\rho_k\left[n\right]\right)p_k\left[n\right]}{\Lambda_k\left[n\right]}\right), \tag{44a}$$

$$\text{s.t.} \quad \underline{\xi}_k\left[n\right]\leq\beta_0\left(u_k\left[n\right]\right)^{-\alpha}+A_k\left[n\right]\left(u\left[n\right]\right)^{-2}+B_k\left[n\right]\left(u_k\left[n\right]\right)^{-\alpha 2}\left(u\left[n\right]\right)^{-1}, \forall k,n, \tag{44b}$$

$$\Lambda_k\left[n\right]\geq\left(1-\rho_k\left[n\right]\right)\sum_{i\neq k}^{K}\psi_{i,k}\left[n\right]p_i\left[n\right]+\frac{\left(1-\rho_k\left[n\right]\right)\sigma_k^2+\delta_k^2}{\underline{\xi}_k\left[n\right]}, \forall n, i\neq k, \tag{44c}$$

$$\rho_k\left[n\right]\left(\sum_{i=1}^{K}p_i\left[n\right]\underline{\xi}_k\left[n\right]+\sigma_k^2\right)\geq\Xi^{-1}\left(\frac{\chi_{th}}{\delta}\right), \forall k,n, \tag{44d}$$

$$\text{(27b)–(27d), (27j), (27k), (35), (36), (40)–(43),} \tag{44e}$$

where $\Xi^{-1}(x) = b_k - \frac{\ln(\xi_k((x+Y_k)X_k)-1)}{a_k}$ and $\Upsilon = \{u_k[n], u[n], \underline{\xi}_k[n], \Lambda_k[n], \pi_i[n], \forall n, i \neq k\}$ denotes the set of all auxiliary variables. It is worth noting that at the solution to the problem $\mathcal{P}2.1$, if any of constraints in (35) and (36) is satisfied with strict inequality, the corresponding $u_k[n]$ or $u[n]$ can be decreased to make (35) and (36) satisfy with equality. Thus, the corresponding $\underline{\xi}_k[n]$ and $\Lambda_k[n]$ can be increased or decreased to make constraint (44b) and (44c) satisfy with equality. Therefore, at the optimal solution to problem $\mathcal{P}2.1$, all constraints must be satisfied with equality, i.e., the problem $\mathcal{P}2$ and $\mathcal{P}2.1$ are equivalent.

Next, we adopt a penalty function-based approach to solve the problem $\mathcal{P}2.1$. By adding (40) as a penalty term to the objective function, the problem $\mathcal{P}2.1$ can be transformed into the problem $\mathcal{P}2.2$ as follows

$$\mathcal{P}2.2: \max_{\mathbf{Q},\boldsymbol{\psi},\Upsilon} \sum_{n=1}^{N}\sum_{k=1}^{K} \log_2\left(1+\frac{(1-\rho_k[n])\,p_k[n]}{\Lambda_k[n]}\right) - \tau_p \sum_{n=1}^{N}\sum_{k=1}^{K}\sum_{i\neq k}^{K} (\psi_{i,k}[n](1-\psi_{i,k}[n])), \tag{45a}$$

$$\text{s.t.} \quad \text{(27b)–(27d), (27j), (27k), (35), (36),}$$
$$\text{(41)–(43), (44b)–(44d),} \tag{45b}$$

where $\tau_p > 0$ denotes the penalty factor, and its role is to penalize the objective function when $\psi_{i,k}$ belongs to 0 to 1. It can be seen that when $\tau_p \to \infty$, the problem $\mathcal{P}2.1$ and the problem $\mathcal{P}2.2$ are equivalent. However, the problem $\mathcal{P}2.2$ is still non-convex optimization problem due to the non-concave objective function and non-convex constraints (35), (36), (43) and (44b). Next, we apply SCA to iteratively obtain a suboptimal solution to problem $\mathcal{P}2.2$.

We define that $f(\Lambda_k[n], \psi_{i,k}[n])$ denotes the objective function of the problem $\mathcal{P}2.2$, which is convex w.r.t $B_k[n]$ and $\psi_{i,k}[n]$. For the r-th iteration of SCA, the lower bound of $f(\Lambda_k[n], \psi_{i,k}[n])$ can be given by (46) shown at the bottom of this page, where $B_k[n]^{(r)}$ and $\psi_{i,k}^{(r)}[n]$ are value of the r-th iteration. Similarly, we can apply SCA to carry out the first-order Taylor expansion of the left-hand-side (LHS) convex functions of constraints (35) and (36), and obtain their lower bounds respectively as following

$$\left(u_k^{(r)}[n]\right)^2 + 2u_k^{(r)}[n]\left(u_k[n]-u_k^{(r)}[n]\right) \geq \|\mathbf{q}[n]-\mathbf{w}_k\|^2, \forall k, n, \tag{47}$$

and

$$\left(u^{(r)}[n]\right)^2 + 2u^{(r)}[n]\left(u[n]-u^{(r)}[n]\right) \geq \|\mathbf{q}[n]-\mathbf{w}_r\|^2, \forall n. \tag{48}$$

Moreover, the non-convex constraint (43) can be rewritten as follows

$$\frac{(\psi_{i,k}[n]+\pi_i[n])^2}{4} - \frac{(\psi_{i,k}[n]-\pi_i[n])^2}{4} \leq \|\mathbf{q}[n]-\mathbf{w}_k\|^2, \forall n, k \neq i. \tag{49}$$

It can be seen that the LHS of the (49) is the difference of the two convex functions w.r.t $\psi_{i,k}[n]$ and $\pi_i[n]$, and the right-hand-side (RHS) is also a convex function w.r.t $\mathbf{q}[n]$. Hence, for the r-th SCA iteration, (49) can be approximately expressed as

$$d_{i,k}^{ub}[n] \leq \left\|\mathbf{q}^{(r)}[n]-\mathbf{w}_k\right\|^2 + 2(\mathbf{q}[n]-\mathbf{w}_k)^T \left(\mathbf{q}[n]-\mathbf{q}^{(r)}[n]\right), \forall n, k \neq i, \tag{50}$$

where

$$d_{i,k}^{ub}[n] = \frac{(\psi_{i,k}[n]+\pi_i[n])^2}{4} + \frac{(\psi_{i,k}^{(r)}[n]-\pi_i^k[n])^2 - 2(\psi_{i,k}^{(r)}[n]-\pi_i^k[n])(\psi_{i,k}[n]-\pi_i[n])}{4}, \forall n, k \neq i.$$

In addition, the RHS of constraint (44b) is intractable due to the AoA in $A_k[n]$ and $B_k[n]$ depend on the UAV location in the n-th time slot $\mathbf{q}[n]$. Herein, we introduce the following constraint

$$\left\|\mathbf{q}[n]-\mathbf{q}^{(r)}[n]\right\|^2 \leq \delta_{\max}^2, \forall n, \tag{51}$$

where $\mathbf{q}^{(r)}[n]$ is the value of the r-th SCA iteration, and $\delta_{\max}$ denotes the maximum allowed displacement of UAV after each SCA iteration. When the value of $\delta_{\max}$ is small enough, we can consider that AoA is approximately unchanged after each SCA iteration. Therefore, $A_k[n]$ and $B_k[n]$ also remain unchanged. The UAV trajectory optimization of the $(r+1)$-th SCA iteration is based on the AoA obtained at the r-th iteration. In order to ensure the accuracy of the approximation, according to [9], we require that the ratio of the maximum allowed deployment of the n-th time slot to the minimum height of the UAV should meet $\delta_{\max}(h_u)_{\min} \leq \varepsilon_{\max}$, i.e., the value of $\delta_{\max}$ under the accuracy

$$f(\Lambda_k[n], \psi_{i,k}[n]) \geq \sum_{n=1}^{N}\sum_{k=1}^{K}\left(\log_2\left(1+\frac{(1-\rho_k[n])\,p_k[n]}{\Lambda_k^{(r)}[n]}\right) - \frac{(1-\rho_k[n])\,p_k[n]\left(\Lambda_k[n]-\Lambda_k^{(r)}[n]\right)}{\Lambda_k^{(r)}[n]\left(\Lambda_k^{(r)}[n]+(1-\rho_k[n])\,p_k[n]\right)\ln 2}\right) - \tau_p\sum_{n=1}^{N}\sum_{k=1}^{K}\sum_{i\neq k}^{K}\left(\psi_{i,k}[n]-\left(\psi_{i,k}^{(r)}[n]\right)^2 - 2\psi_{i,k}^{(r)}[n]\left(\psi_{i,k}[n]-\psi_{i,k}^{(r)}[n]\right)\right) \triangleq f(\Lambda_k[n], \psi_{i,k}[n])^{lb}, \tag{46}$$

threshold $\varepsilon_{\max}$ can be represented by $\delta_{\max} \leq (h_u)_{\min}\varepsilon_{\max}$.[3] Accordingly, the RHS of constraint (44b) only depends on $u_k[n]$ and $u[n]$. We use the following lemma to deal with constraint (44b).

Lemma 2: For given $a_1 > 0, a_2 > 0$ and $a_3 > 0$, $g_1(x_1, x_2) = a_1(x_1)^{-\alpha} + a_2(x_2)^{-2}$ and $g_2(x_1, x_2) = a_3(x_1)^{-\alpha 2}(x_2)^{-1}$ are both convex jointly w.r.t. $x_1 > 0$ and $x_2 > 0$. ■

Proof: By proving that when $x_1 > 0$ and $x_2 > 0$, the Hessian matrices of $g_1(x_1, x_2)$ and $g_2(x_1, x_2)$ are positive semi-definite, therefore, both are convex functions. The proof of Lemma 2 is completed.

Let $\tilde{g} = \beta_0(u_k[n])^{-\alpha} + A_k[n](u[n])^{-2}$ and $\tilde{h} = (u_k[n])^{-\alpha 2}(u[n])^{-1}$. The RHS of the (44b) can be given by $\tilde{g} + B_k[n]\tilde{h}$. Since $\beta_0 > 0$, if $B_k > 0$, then $\tilde{g} + |B_k[n]|\tilde{h}$ is convex jointly w.r.t. $u_k[n]$ and $u[n]$ according to Lemma 2. Otherwise, $\tilde{g} - |B_k[n]|\tilde{h}$ is the difference between the two convex functions. Thus, constraint (44b) is non-convex. Given the value of the r-th iteration $u_k^{(r)}[n]$ and $u^{(r)}[n]$, we apply SCA to obtain the lower bound of $\tilde{g} + B_k[n]\tilde{h}$, which can be given by

$$\left(\tilde{g} + B_k[n]\,\tilde{h}\right)^{lb} = \begin{cases} \tilde{g}^{lb} + |B_k[n]|\,\tilde{h}^{lb} \\ \tilde{g}^{lb} - |B_k[n]|\,\tilde{h} \end{cases}. \tag{52}$$

where $\tilde{g}^{lb}$ and $\tilde{h}^{lb}$ are as follows.

$$\begin{aligned} \tilde{g}^{lb} = {} & \beta_0\left(u_k^{(r)}[n]\right)^{-\alpha} - \alpha\left(u_k^{(r)}[n]\right)^{-\alpha-1}\left(u_k[n] - u_k^{(r)}[n]\right) \\ & + A_k[n]\left(u^{(r)}[n]\right)^{-2} - 2A_k[n]\left(u^{(r)}[n]\right)^{-3} \\ & \times \left(u[n] - u^{(r)}[n]\right), \forall k, n, \end{aligned} \tag{53}$$

and

$$\begin{aligned} \tilde{h}^{lb} = {} & \left(u_k^{(r)}[n]\right)^{-\alpha 2}\left(u^{(r)}[n]\right)^{-1} - \frac{\alpha}{2}\left(u_k^{(r)}[n]\right)^{-\alpha 2-1} \\ & \times \left(u^{(r)}[n]\right)^{-1}\left(u_k[n] - u_k^{(r)}[n]\right) - \left(u_k^{(r)}[n]\right)^{-\alpha 2} \\ & \times \left(u^{(r)}[n]\right)^{-2}\left(u[n] - u^{(r)}[n]\right), \forall k, n, \end{aligned} \tag{54}$$

Therefore, constraint (44b) can be transformed into

$$\underline{\xi}_k[n] \leq \left(\tilde{g} + B_k[n]\,\tilde{h}\right)^{lb}, \forall k, n. \tag{55}$$

Accordingly, the problem $\mathcal{P}2.2$ can be transformed into the problem $\mathcal{P}2.3$, which can be expressed as

$$\mathcal{P}2.3: \quad \max_{\mathbf{Q},\boldsymbol{\psi},\Upsilon} f(\Lambda_k[n], \psi_{i,k}[n])^{lb}, \tag{56a}$$

$$\text{s.t.} \quad \text{(27b)–(27d), (27j), (27k), (41), (42),}$$
$$\text{(44c), (44d), (47), (48), (50), (55).} \tag{56b}$$

The problem $\mathcal{P}2.2$ is a standard convex optimization problem, which can be solved by using the standard solvers, e.g., CVX toolbox [37].

[3]It is worth noting that a sufficiently small $\varepsilon_{\max}$ will improve the accuracy of the approximation, but it will also increase the computational complexity. Therefore, the choice of a suitable $\varepsilon_{\max}$ can well balance the relationship between accuracy and complexity.

C. Optimization of PS Ratio $\boldsymbol{\rho}$

For given UAV trajectory $\mathbf{Q}$, SIC decoding order $\boldsymbol{\psi}$, UAV transmit power allocation $\mathbf{p}$, and IRS reflection coefficient $\boldsymbol{\theta}$, the user PS ratio $\boldsymbol{\rho}$ optimization problem can be transformed into the problem $\mathcal{P}3$, which can be expressed as

$$\mathcal{P}3: \quad \max_{\boldsymbol{\rho}} \sum_{n=1}^{N}\sum_{k=1}^{K} \tilde{R}_k[n], \tag{57a}$$

$$\text{s.t.} \quad \text{(27h)}, \tag{57b}$$

$$\rho_k[n]\left(\sum_{i=1}^{K} p_i[n]\,\xi_k[n] + \sigma_k^2\right) \geq \Xi^{-1}\left(\frac{\chi_{th}}{\delta}\right), \forall k, n. \tag{57c}$$

It can be proved that the objective function $\tilde{R}_k[n]$ is concave w.r.t $\rho_k[n]$, and it is omitted here. Hence, the problem $\mathcal{P}3$ is a standard convex optimization problem, which can be solved by using CVX toolbox [37].

D. Optimization of UAV Transmit Power Allocation $\mathbf{p}$

For given UAV trajectory $\mathbf{Q}$, SIC decoding order $\boldsymbol{\psi}$, user PS ratio $\boldsymbol{\rho}$, and IRS reflection coefficient $\boldsymbol{\theta}$, the UAV transmit power allocation $\mathbf{p}$ optimization problem can be expressed as

$$\mathcal{P}4: \quad \max_{\mathbf{p}} \sum_{n=1}^{N}\sum_{k=1}^{K} \tilde{R}_k[n], \tag{58a}$$

$$\text{s.t.} \quad \text{(27e), (27f), (27k)}, \tag{58b}$$

$$\rho_k[n]\left(\sum_{i=1}^{K} p_i[n]\,\xi_k[n] + \sigma_k^2\right) \geq \Xi^{-1}\left(\frac{\chi_{th}}{\delta}\right), \forall k, n. \tag{58c}$$

The problem $\mathcal{P}4$ is a non-convex optimization problem due to the non-concave objective function. The objective function of the problem $\mathcal{P}4$ can be further expressed as

$$\begin{aligned} \tilde{R}_k[n] = {} & \underbrace{\log_2\left((1-\rho_k[n])\left(\sum_{i=1}^{K}\psi_{i,k}[n]\,p_i[n]\,\xi_k[n] + \sigma_k^2\right) + \delta_k^2\right)}_{\bar{\ell}_{i,k}[n]} \\ & \underbrace{- \log_2\left((1-\rho_k[n])\left(\sum_{i\neq k}^{K}\psi_{i,k}[n]\,p_i[n]\,\xi_k[n] + \sigma_k^2\right) + \delta_k^2\right)}_{\tilde{\ell}_{i,k}[n]}, \\ & \forall n, k \neq i. \end{aligned} \tag{59}$$

For the convenience of analysis, we set $\psi_{i,i}[n] = 1$. $\tilde{R}_k[n]$ is non-concave w.r.t. $p_i[n]$ due to it is a form of difference of concave functions. Thus, we apply SCA to obtain the upper bound of

$\tilde{\ell}_{i,k}[n]$ on the RHS of (59) as follows

$$\tilde{\ell}_{i,k}[n] \le \tilde{\ell}_{i,k}[n]\left(p_i^{(r)}[n]\right) + \frac{\sum_{i\neq k}^{K}\psi_{i,k}[n]\,\xi_k[n]\left(p_i[n]-p_i^{(r)}[n]\right)}{\left((1-\rho_k[n])\left(\sum_{i\neq k}^{K}\psi_{i,k}[n]\,p_i^{(r)}[n]\,\xi_k[n]+\sigma_k^2\right)+\delta_k^2\right)\ln 2} \triangleq \left(\tilde{\ell}_{i,k}[n]\right)^{ub}, \forall n, k\neq i, \tag{60}$$

where $p_i^{(r)}[n]$ is value of the r-th SCA iteration. Accordingly, the problem $\mathcal{P}4$ can be transformed into the problem $\mathcal{P}4.1$, which can be given by

$$\mathcal{P}4.1: \max_{\mathbf{p}} \sum_{n=1}^{N}\sum_{k=1}^{K}\left(\bar{\ell}_{i,k}[n]-\left(\tilde{\ell}_{i,k}[n]\right)^{ub}\right), \tag{61a}$$

$$\text{s.t.} \quad (27e),\ (27f),\ (27k), \tag{61b}$$

$$\rho_k[n]\left(\sum_{i=1}^{K}p_i[n]\,\xi_k[n]+\sigma_k^2\right)\ge\Xi^{-1}\left(\frac{\chi_{th}}{\delta}\right), \quad \forall k,n. \tag{61c}$$

It can be seen that the problem $\mathcal{P}4.1$ is a standard convex optimization problem, which can be solved by applying CVX toolbox [37].

E. Optimization of IRS Reflection Coefficient $\boldsymbol{\theta}$

For given UAV trajectory $\mathbf{Q}$, user PS ratio $\boldsymbol{\rho}$, and UAV transmit power allocation $\mathbf{p}$, the IRS reflection coefficient $\boldsymbol{\theta}$ optimization problem can be expressed as

$$\mathcal{P}5: \max_{\boldsymbol{\theta}} \tilde{R}_{\text{sum}}, \tag{62a}$$

$$\text{s.t.} \quad (27g),\ (27l). \tag{62b}$$

The problem $\mathcal{P}5$ is non-convex due to the non-concave objective function and non-convex constraint (27g) and (27l). We introduce auxiliary variables $\mathbf{a}_k^H[n]=\widehat{\mathbf{h}}_{\text{IU},k}^H\text{diag}(\mathbf{h}_{\text{UI}}[n])\in\mathbb{C}^{1\times M},\forall k,n$ and $\mathbf{b}[n]=[e^{j\theta_1[n]},\ldots,e^{j\theta_M[n]}]^T\in\mathbb{C}^{M\times 1}$. Thus, the (25) can be written as follows

$$\xi_k[n]=\varpi_k[n]+\left|\mathbf{a}_k^H[n]\,\mathbf{b}[n]\right|^2, \forall k,n, \tag{63}$$

where $\varpi_k[n]=\frac{\beta_0-\vartheta_1}{(d_{\text{UU},k}[n])^{\alpha}}+\frac{M\beta_0(\beta_0-\vartheta_2)}{(d_{\text{UI}}[n])^2(d_{\text{IU},k})^{\gamma}}$. Let $\mathbf{A}_k[n]=\mathbf{a}_k[n]\mathbf{a}_k^H[n]\in\mathbb{C}^{M\times M}$ and $\mathbf{B}[n]=\mathbf{b}[n]\mathbf{b}[n]^H\in\mathbb{C}^{M\times M}$. They satisfy $\text{rank}(\mathbf{A}_k[n])=1$ and $\text{rank}(\mathbf{B}[n])=1$. Then (63) can be further expressed as

$$\xi_k[n]=\varpi_k[n]+\text{tr}\left(\mathbf{A}_k[n]\,\mathbf{B}[n]\right). \tag{64}$$

Hence, the (30) can be rewritten as the (65) shown at the bottom of this page. Next, we can apply DC programming to transform the non-convex constraint $\text{rank}(\mathbf{B}[n])=1$.

Proposition 1: For the positive semi-definite matrix $\mathbf{M}\in\mathbb{C}^{N\times N}$, $\text{tr}(\mathbf{M})>0$, the rank-one constraint can be expressed as the difference between two convex functions, i.e.,

$$\text{rank}(\mathbf{M})=1 \Leftrightarrow \text{tr}(\mathbf{M})-\|\mathbf{M}\|_2=0, \tag{66}$$

where $\text{tr}(\mathbf{M})=\sum_{n=1}^{N}\sigma_n(\mathbf{M})$, $\|\mathbf{M}\|_2=\sigma_1(\mathbf{M})$ is spectral norm, and $\sigma_n(\mathbf{M})$ represents the n-th largest singular value of matrix $\mathbf{M}$ [38].

According to $\mathbf{Proposition1}$, we transform the non-convex rank-one constraint on matrix $\mathbf{B}[n]$, and then add it as a penalty term to the objective function of problem $\mathcal{P}5$. Therefore, problem $\mathcal{P}5$ can be transformed into

$$\mathcal{P}5.1: \max_{\mathbf{B}[n]} \sum_{n=1}^{N}\sum_{k=1}^{K}(\bar{\iota}_{i,k}[n]-\tilde{\iota}_{i,k}[n])-\varsigma_p(\text{tr}(\mathbf{B}[n])-\|\mathbf{B}[n]\|_2), \tag{67a}$$

$$\text{s.t.} \quad \rho_k[n]\left(\sum_{i=1}^{K}p_i[n]\left(\varpi_k[n]+\text{tr}\left(\mathbf{A}_k[n]\,\mathbf{B}[n]\right)\right)+\sigma_k^2\right) \ge \Xi^{-1}\left(\frac{\chi_{th}}{\delta}\right), \forall k,n, \tag{67b}$$

$$\mathbf{B}[n]_{m,m}=1, \forall m,n, \tag{67c}$$

$$\mathbf{B}[n]\succeq 0, \forall n, \tag{67d}$$

where $\varsigma_p>0$ denotes the penalty factor related to the rank-one constraint. It can be seen that when $\varsigma_p\to\infty$, the problem $\mathcal{P}5.1$ and the problem $\mathcal{P}5$ are equivalent. The problem $\mathcal{P}5.1$ is still non-convex optimization problem due to the objective function is non-concave. As $\tilde{\iota}_{i,k}[n]$ is concave w.r.t $\mathbf{B}[n]$, the upper bound can be obtained by adopting SCA as follows

$$\tilde{\iota}_{i,k}[n]\le\tilde{\iota}_{i,k}[n]\left(\mathbf{B}^{(r)}[n]\right)+\text{tr}\left(\left(\nabla_{\mathbf{B}^{(r)}[n]}\tilde{\iota}_{i,k}[n]\left(\mathbf{B}^{(r)}[n]\right)\right)^H\left(\mathbf{B}[n]-\mathbf{B}^{(r)}[n]\right)\right)\triangleq(\tilde{\iota}_{i,k}[n])^{ub}, \forall n,k\neq i, \tag{68}$$

$$\tilde{R}_k[n]=\underbrace{\log_2\left((1-\rho_k[n])\sum_{i=1}^{K}\psi_{i,k}[n]\,p_i[n]\,\text{tr}\left(\mathbf{A}_k[n]\,\mathbf{B}[n]\right)+\bar{v}_k[n]\right)}_{\bar{\iota}_{i,k}[n]} - \underbrace{\log_2\left((1-\rho_k[n])\sum_{i\neq k}^{K}\psi_{i,k}[n]\,p_i[n]\,\text{tr}\left(\mathbf{A}_k[n]\,\mathbf{B}[n]\right)+\tilde{v}_k[n]\right)}_{\tilde{\iota}_{i,k}[n]}, \forall n,k\neq i, \tag{65}$$

where $\nabla_{\mathbf{B}^{(r)}[n]}\tilde{\iota}_{i,k}[n](\mathbf{B}^{(r)}[n])$ is denoted by (69) shown at the bottom of this page. In addition, since $\|\mathbf{B}[n]\|_2$ is a convex function, we can also adopt SCA to obtain its lower bound as follows

$$\|\mathbf{B}[n]\|_2 \geq \left\|\mathbf{B}^{(r)}[n]\right\|_2 + \mathrm{tr}\left(\mathbf{u}_{\max}\left(\mathbf{B}^{(r)}[n]\right)\mathbf{u}_{\max}\left(\mathbf{B}^{(r)}[n]\right)^H \left(\mathbf{B}[n]-\mathbf{B}^{(r)}[n]\right)\right) \triangleq \left(\|\mathbf{B}[n]\|_2\right)^{lb}, \forall n, \tag{70}$$

where $\mathbf{u}_{\max}(\mathbf{B}^{(r)}[n])$ denotes the eigenvector corresponding to the largest singular value of the matrix $\mathbf{B}^{(r)}[n]$. Therefore, the non-convex problem $\mathcal{P}5.1$ can be approximately transformed into

$$\mathcal{P}5.2: \sum_{n=1}^{N}\sum_{k=1}^{K}\left(\bar{\iota}_{i,k}[n]-\left(\tilde{\iota}_{i,k}[n]\right)^{ub}\right) - \varsigma_p\left(\mathrm{tr}\left(\mathbf{B}[n]\right)-\left(\|\mathbf{B}[n]\|_2\right)^{lb}\right), \tag{71a}$$

$$\text{s.t.} \quad (67b)\text{–}(67d). \tag{71b}$$

It can be seen that the problem $\mathcal{P}5.2$ is a standard SDP problem, which can be solved by using CVX toolbox [37].

F. Computational Complexity and Convergence Analysis

1) Computational Complexity Analysis: In each iteration, the problem $\mathcal{P}2.3$ is solved with the computational complexity of $\mathcal{O}(N^{3.5}+KN)$, the problem $\mathcal{P}3$ and problem $\mathcal{P}4.1$ both are solved with computational complexity of $\mathcal{O}(KN^{3.5})$. The problem $\mathcal{P}5.2$ solves a SDP problem by interior point method, so the computational complexity can be represented by $\mathcal{O}(M^{3.5})$ [39]. We assume that the number of iterations required for the algorithm to reach convergence is r, the computational complexity of the proposed algorithm can be expressed as $\mathcal{O}(r(N^{3.5}+KN+(KN)^{3.5}+M^{3.5}))$.

2) Convergence Analysis: The convergence of the proposed joint UAV trajectory, SIC decoding order, UAV transmit power allocation, PS ratio and IRS reflection coefficient optimization in IRS empowered UAV SWIPT networks can be elaborated as follows.

We define $\mathbf{Q}^{(r)}$, $\boldsymbol{\psi}^{(r)}$, $\boldsymbol{\rho}^{(r)}$, $\mathbf{p}^{(r)}$ and $\boldsymbol{\theta}^{(r)}$ as the r-th iteration solution of the problem $\mathcal{P}2.3$, $\mathcal{P}3$, $\mathcal{P}4.1$ and $\mathcal{P}5.2$. Herein, the objective function is denoted by $\Re(\mathbf{Q}^{(r)}, \boldsymbol{\psi}^{(r)}, \boldsymbol{\rho}^{(r)}, \mathbf{p}^{(r)}, \boldsymbol{\theta}^{(r)})$. In the step 3 of Algorithm 1, since the UAV trajectory and SIC decoding order can be obtained for given $\boldsymbol{\rho}^{(r)}$, $\mathbf{p}^{(r)}$ and $\boldsymbol{\theta}^{(r)}$. Hence, we have

$$\Re\left(\mathbf{Q}^{(r)}, \boldsymbol{\psi}^{(r)}, \boldsymbol{\rho}^{(r)}, \mathbf{p}^{(r)}, \boldsymbol{\theta}^{(r)}\right) \leq \Re\left(\mathbf{Q}^{(r+1)}, \boldsymbol{\psi}^{(r+1)}, \boldsymbol{\rho}^{(r)}, \mathbf{p}^{(r)}, \boldsymbol{\theta}^{(r)}\right). \tag{72}$$

Similarly, in the step 4 of Algorithm 1, we can obtain the user PS ratio when $\mathbf{Q}^{(r+1)}$, $\boldsymbol{\psi}^{(r+1)}$, $\mathbf{p}^{(r)}$ and $\boldsymbol{\theta}^{(r)}$ are given. Herein, we also have

$$\Re\left(\mathbf{Q}^{(r+1)}, \boldsymbol{\psi}^{(r+1)}, \boldsymbol{\rho}^{(r)}, \mathbf{p}^{(r)}, \boldsymbol{\theta}^{(r)}\right) \leq \Re\left(\mathbf{Q}^{(r+1)}, \boldsymbol{\psi}^{(r+1)}, \boldsymbol{\rho}^{(r+1)}, \mathbf{p}^{(r)}, \boldsymbol{\theta}^{(r)}\right). \tag{73}$$

In the step 5 of Algorithm 1, UAV transmit power allocation can be obtained when $\mathbf{Q}^{(r+1)}$, $\psi^{(r+1)}$, $\boldsymbol{\rho}^{(r+1)}$ and $\boldsymbol{\theta}^{(r)}$ are given. Therefore, we have

$$\Re\left(\mathbf{Q}^{(r+1)}, \boldsymbol{\psi}^{(r+1)}, \boldsymbol{\rho}^{(r+1)}, \mathbf{p}^{(r)}, \boldsymbol{\theta}^{(r)}\right) \leq \Re\left(\mathbf{Q}^{(r+1)}, \boldsymbol{\psi}^{(r+1)}, \boldsymbol{\rho}^{(r+1)}, \mathbf{p}^{(r+1)}, \boldsymbol{\theta}^{(r)}\right). \tag{74}$$

Finally, in the step 6 of Algorithm 1, IRS reflection coefficient can be obtained when $\mathbf{Q}^{(r+1)}$, $\psi^{(r+1)}$, $\boldsymbol{\rho}^{(r+1)}$ and $\mathbf{p}^{(r+1)}$ are fixed. Therefore, we have

$$\Re\left(\mathbf{Q}^{(r+1)}, \boldsymbol{\psi}^{(r+1)}, \boldsymbol{\rho}^{(r+1)}, \mathbf{p}^{(r+1)}, \boldsymbol{\theta}^{(r)}\right) \leq \Re\left(\mathbf{Q}^{(r+1)}, \boldsymbol{\psi}^{(r+1)}, \boldsymbol{\rho}^{(r+1)}, \mathbf{p}^{(r+1)}, \boldsymbol{\theta}^{(r+1)}\right). \tag{75}$$

Based on the above, we can obtain

$$\Re\left(\mathbf{Q}^{(r)}, \boldsymbol{\psi}^{(r)}, \boldsymbol{\rho}^{(r)}, \mathbf{p}^{(r)}, \boldsymbol{\theta}^{(r)}\right) \leq \Re\left(\mathbf{Q}^{(r+1)}, \boldsymbol{\psi}^{(r+1)}, \boldsymbol{\rho}^{(r+1)}, \mathbf{p}^{(r+1)}, \boldsymbol{\theta}^{(r+1)}\right). \tag{76}$$

which shows that the value of the objective function is non-decreasing after each iteration of Algorithm 1. Since the objective function is upper bounded by a finite value due to the limited transmit power of UAV, the convergence of Algorithm 1 can be guaranteed.

IV. Numerical Results

In this section, we verify the effectiveness of the proposed algorithm through the numerical results. In this paper, we consider that $K=6$ ground users are randomly distributed in a 500×500 circular area. We assume that the UAV flies at a fixed height $h_u = 100$ m, and its maximum flight speed $V_{max} = 20$ m/s. The maximum transmit power of UAV is $P_{max} = 43$ dBm. The coordinates of the initial horizontal position and final horizontal position of the UAV are (0, 250) and (500, 250), respectively. In addition, we consider that the IRS is fixed on a building with a height of $h_r = 30$ m, and its horizontal position coordinate is (250, 0). The number of IRS reflecting elements is $M=20$. The channel power gain at when the reference distance $d_0 = 1$ m is $\beta_0 = $ -30 dB. We assume that the parameters of all users are the same, i.e., $\xi_k = 24\mathrm{mW}$, $a_k = 150$ and $b_k = 0.024$ [40]. The Rice factor is $\kappa_1 = \kappa_2 = = 3$ dB. The additive white

$$\nabla_{\mathbf{B}^{(r)}[n]}\tilde{\iota}_{i,k}[n]\left(\mathbf{B}^{(r)}[n]\right) = \frac{(1-\rho_k[n])\,\mathbf{A}_k^H[n]\sum_{i\neq k}^{K}\psi_{i,k}[n]\,p_i[n]}{\left((1-\rho_k[n])\sum_{i\neq k}^{K}\psi_{i,k}[n]\,p_i[n]\,\mathrm{tr}\left(\mathbf{A}_k[n]\,\mathbf{B}^{(r)}[n]\right)+\tilde{v}_k[n]\right)\ln 2}, \forall n, k\neq i. \tag{69}$$

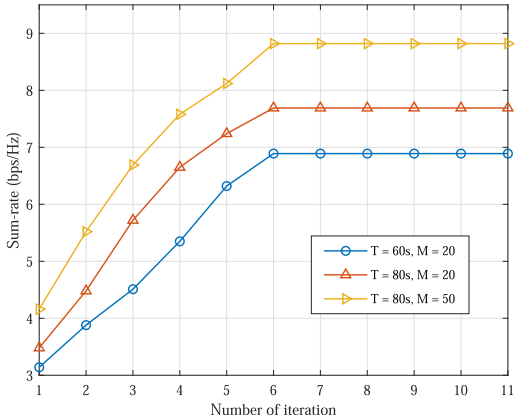

Fig. 3. Convergence behaviour of the proposed optimization algorithm.

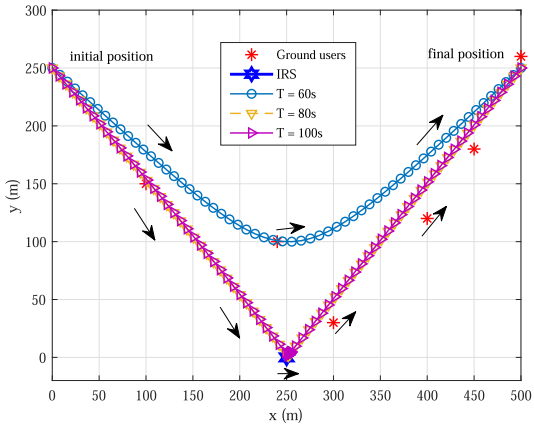

Fig. 4. UAV optimization trajectory at different time periods T assisted by IRS.

Gaussian noise of the transmission channel is $\sigma = -80$ dBm. The path loss exponents of the UU-channel and IU-channel are $\alpha = \gamma = 2.2$. In addition, we set $\epsilon_m ax = 0.1$ and $\delta_{\max} = 5$ m. The threshold of proposed algorithm is set as 10^{-3}. In addition, the initialization method of the optimization variables is as follows: For the initialization of the user PS ratio, we make it randomly generated within $[0, 1]$. The initial value of the IRS reflection coefficient is randomly generated within $[0, 2\pi)$. The UAV transmit power is initialized by using an equal allocation scheme. The initial value of the UAV's trajectory is the position where the UAV is randomly generated in the coordinate plane in each time slot n, and the SIC decoding order is generated depending on the distance between the user and the UAV.

We first evaluate the convergence of the proposed algorithm. Fig. 3 shows the change of sum-rate with the number of iteration under different time periods T and different IRS reflection elements M. We can see that the sum-rate increases rapidly with the number of iteration and can reach stable convergence in about six iterations, which verifies the convergence of the proposed algorithm. It can also be seen that when the IRS reflection elements are the same, a larger time duration T can bring a larger system performance gain. Similarly, when the time duration T is the same, more IRS reflection elements can also increase the system sum-rate.

Next, we elaborate the optimized trajectory of UAV at different time periods T assisted by IRS in Fig. 4. From Fig. 4, we can see that when the time period T is larger, UAV can be closer to more ground users, and can provide better wireless information transmission and wireless energy transmission. With the assistance of IRS, UAV can fly to IRS to balance the channel conditions of UU-channel and combined channels to provide better quality-of-service (QoS) for ground users. In addition, when the time period T is large enough, the UAV can spend more time staying near the IRS to provide higher quality services for ground users.

Then, we compare the proposed algorithm with several other benchmark algorithms as follows: (1) Benchmark 1 (Equ-power): UAV transmit power allocation adopts the scheme of equal allocation. The optimization scheme for other variables is the same as Algorithm 1. (2) Benchmark 2 (No-opt-trajectory): The UAV trajectory is not optimized, and a random scheme is used. The optimization scheme for other variables is the same as Algorithm 1. (3) Benchmark 3 (No-opt-phase): The IRS phase shift is not optimized and a random phase shift is used. The optimization scheme for other variables is the same as Algorithm 1. (4) Benchmark 4 (Com-opt): All optimization variables are optimized only once using the optimization algorithm for each sub-problem in Algorithm 1, and no alternate optimization is performed. (5) Benchmark 5 (Ran-opt): All optimization variables are random. (6) Benchmark 6 (Static-opt): Optimize the deployment of static UAV. (7) Benchmark 7 (Static-ran): Random deployment of static UAV. For benchmark 6 and benchmark 7, the optimization for other variables is the same as the proposed algorithm 1 except that UAV trajectory optimization is not considered. They consider the static deployment problem of UAV. Benchmark 6 considers the UAV to be deployed at a random position in the circular area, and benchmark 7 uses the exhaustive method to find the sub-optimal deployment position of the circular area after optimizing other variables. (8) Benchmark 8 (Non-max-rate): UAV without maximum flight rate constraint. (9) Benchmark 9 (Str-trajectory): UAV flies in a straight line from the initial position to the final position. (10) No-IRS: Without the assistance of IRS, the optimization algorithm for other variables is the same as Algorithm 1.

Fig. 5 shows the variation of the system sum-rate with the number of IRS reflection elements for the proposed algorithm and benchmark algorithms. It can be seen that when the number of IRS reflection elements increases, the performance of the proposed algorithm improves. This is because the number of IRS reflection elements increases, the number of combined channels will also increase, which can provide better channel quality for ground users, i.e., the sum-rate will also increase accordingly. Compared with other benchmark algorithms, our proposed algorithm has obvious performance gains. Specifically, when the number of IRS reflection elements is the same, the performance of the proposed algorithm is better than that of benchmark 1, which is mainly due to the fact that in benchmark 1, the UAV transmit power is not optimized, but an equal allocation scheme is adopted. Similarly, the main reason why the proposed algorithm outperforms benchmark 2 and benchmark 3 is that

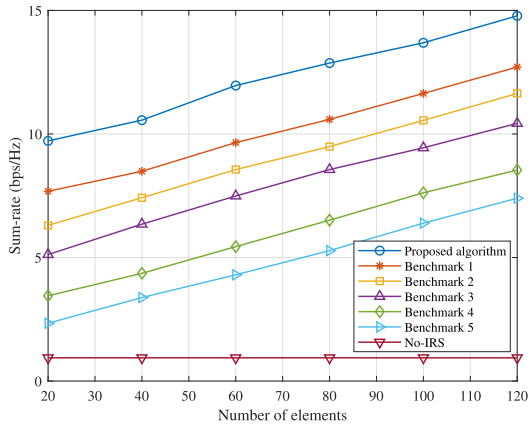

Fig. 5. Sum-rate versus the number of IRS reflection elements for the proposed algorithm and different benchmark algorithms.

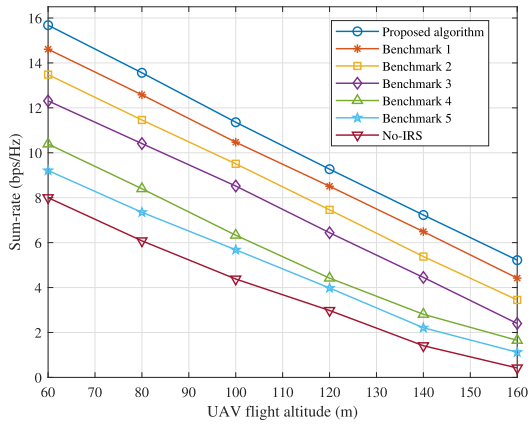

Fig. 6. Sum-rate versus the UAV flight altitude for the proposed algorithm and different benchmark algorithms.

the latter two are not optimized for the UAV trajectory and the phase shift of IRS, respectively. In addition, the performance of benchmark 2 is better than that of benchmark 3, indicating that the gain of the proposed algorithm mainly comes from the phase shift optimization of IRS. This is because if the phase shift setting of the IRS is unreasonable, it is likely to deteriorate the system performance. Moreover, the performance of the proposed algorithm is better than benchmark 4, mainly because benchmark 4 does not have alternate optimization to achieve global convergence. Benchmark 5 has the worst performance due to its random scheme. Finally, it can be seen that in terms of system performance, the IRS-assisted system has a larger gain than the non-IRS-assisted system, because the IRS can improve the system performance by increasing the directional beam. Therefore, it is practical to improve the performance of conventional UAV SWIPT network by this low-cost passive IRS.

In Fig. 6, we compare the change of sum-rate with the UAV height h_u for the proposed algorithm and benchmark algorithms. It describes that when the height of the UAV increases, the system sum-rate decreases. This is mainly due to when the UAV is close to the ground users, the quality of the air-ground channel provided can be improved, thus the user's rate can also

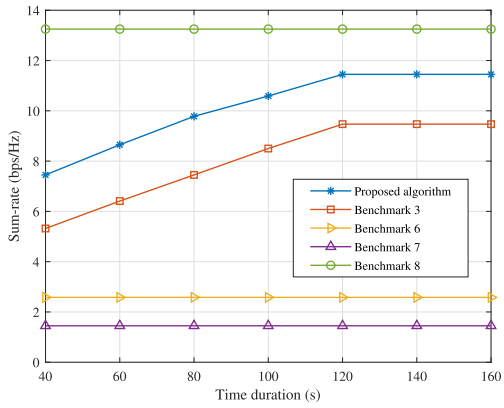

Fig. 7. Sum-rate versus time period T for the proposed algorithm and benchmark algorithms.

be increased, thereby enhancing the system sum-rate. When the height of the UAV is the same, the performance of our proposed algorithm still has a significant performance gain. The reasons for generating the gain are similar to those mentioned above, and will not be repeated here.

Fig. 7 shows the effect of UAV on system sum-rate with dynamic flight and static deployment. It can be seen that compared with benchmark 7, benchmark 6 has better performance in terms of sum-rate. Moreover, the proposed algorithm considers the UAV's optimized trajectory, i.e., the UAV can fly dynamically and serve as many ground users as possible. Therefore, the performance of the proposd algorithm has a significant gain compared to benchmark 6 and benchmark 7. In addition, benchmark 3 considers the equal allocation of UAV transmit power, i.e., for all users to distribute the same power, the rate of users farther from UAV will be reduced. Therefore, the proposed algorithm considering UAV power allocation optimization has a gain in terms of sum-rate compared to benchmark 3. Next, we consider the case that the UAV without maximum flight rate constraint, i.e., benchmark 8. In benchmark 8, the UAV can hover directly above each ground user long enough without considering the flight rate constraints, and then fly to the next user, which can significantly improve the throughput of ground users. Therefore, compared with the proposed algorithm, the performance of this algorithm in terms of sum-rate is better. However, in practical scenarios, UAV usually has a maximum flight rate constraint. In summary, the proposed algorithm is closer to the practical setup and has a higher performance gain compared to several benchmark algorithms.

Next, Fig. 8 illustrates the effect of different UAV trajectory schemes in terms of sum-rate. benchmark 8 has been mentioned above, here we can understand it as a UAV trajectory scheme, i.e., UAV provides services to ground users through hover-flight. UAV flies directly above each user to provide services, and then flies to another user. Therefore, compared to the proposed algorithm, the rate of each user can be improved, thereby the system sum-rate can be improved. In benchmark 9, UAV does not fly according to the user's position, and not all users' rates are guaranteed well, so the system sum-rate will decrease compared to the proposed algorithm.

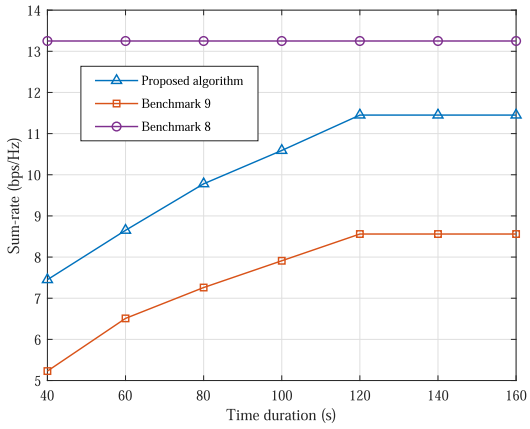

Fig. 8. Sum-rate versus time period T for the proposed algorithm and different UAV trajectory designs.

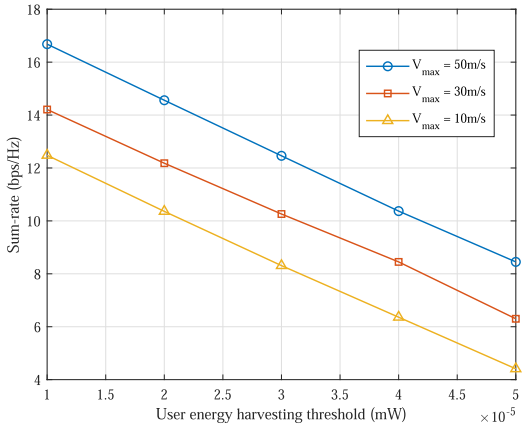

Fig. 10. Sum-rate versus user energy harvesting threshold with different UAV maximum flight speed.

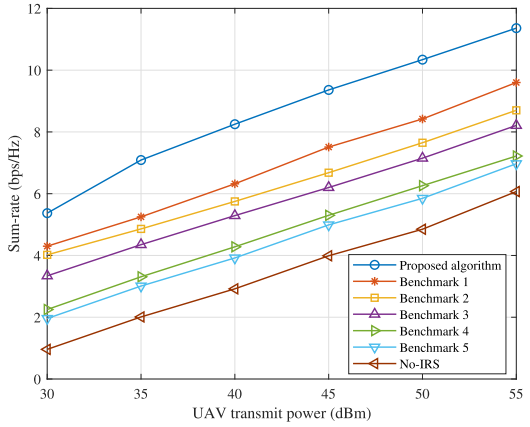

Fig. 9. Sum-rate versus UAV maximum transmit power for the proposed algorithm and benchmark algorithms.

In Fig. 9, the sum-rate versus UAV maximum transmit power for the proposed algorithm and benchmark algorithms is shown. It can be seen that when the UAV maximum transmit power increases, the sum-rate will also increase, which can be explained as the increase of the UAV transmit power, the rate of all users can be improved, so sum-rate of system will also increase. In addition, the performance of our proposed algorithm is superior to the benchmark algorithms, mainly because we consider the joint optimization of all variables and achieve the convergence of the problem by applying AO technique.

Finally, in Fig. 10, we depict the change of sum-rate with the user energy harvesting threshold under different UAV maximum flight speed. It can be seen from Fig. 10 that when the user energy harvesting threshold is fixed, the maximum flight speed of UAV has an impact on the system sum-rate, i.e., the sum-rate increases as the UAV maximum flight rate increases. This is because the greater the UAV maximum flight speed, the longer UAV can hover at the user, so it can provide better QoS for the users. In addition, considering the SWIPT architecture in this paper, the change of sum-rate with the energy harvesting threshold of ground users reflects the trade-off in the IRS-empowered UAV SWIPT networks. When the user energy harvesting threshold continues to increase, i.e., the user's energy requirement becomes greater, the sum-rate of system will gradually decrease. The main reason is that the increase in energy requirements of ground users triggers the power splitting ratio to use more power resources of UAV for wireless energy transmission and a smaller portion for wireless information transmission, which leads to a reduction in the rate of ground users, thereby the system sum-rate will decrease.

V. Conclusion

This paper investigates the sum-rate maximization problem of IRS empowered UAV SWIPT networks. Specifically, under the constraints of the energy harvesting threshold, UAV trajectory, SIC decoding order, UAV transmit power allocation, PS ratio and IRS reflection coefficient are jointly optimized. First, we transform the problem into a tractable problem. Then, in order to solve the transformed problem, we apply the AO algorithm framework to divide the original problem into four sub-problems for solving. Specifically, when the other three sets of variables are given, we apply SCA, penalty function method and DC programming to alternately optimize the optimization variables until convergence is achieved. Then, the computational complexity and convergence analysis of the proposed algorithm is given. Finally, the numerical simulation results verify the convergence and effectiveness of the algorithm, which shows that the proposed algorithm can significantly improve the sum-rate of the system, and the role of IRS is extremely important, and the system performance can be improved at a lower cost, which is very meaningful.

References

[1] D. Xu and H. Zhu, "Secure transmission for SWIPT IoT systems with full-duplex IoT devices," *IEEE Internet Things J.*, vol. 6, no. 6, pp. 10915–10933, Dec. 2019.

[2] G. Bedi, G. K. Venayagamoorthy, R. Singh, R. R. Brooks, and K.-C. Wang, "Review of Internet of Things (IoT) in electric power and energy systems," *IEEE Internet Things J.*, vol. 5, no. 2, pp. 847–870, Apr. 2018.

[3] J. Wang, C. Jiang, Z. Han, Y. Ren, and L. Hanzo, "Internet of vehicles: Sensing-aided transportation information collection and diffusion," *IEEE Trans. Veh. Technol.*, vol. 67, no. 5, pp. 3813–3825, May 2018.

[4] A. Li and C. Masouros, "Energy-efficient SWIPT: From fully digital to hybrid analogdigital beamforming," *IEEE Trans. Veh. Technol.*, vol. 67, no. 4, pp. 3390–3405, Apr. 2018.
[5] H. Cao, Z. Li, and W. Chen, "Resource allocation for IRS-assisted wireless powered communication networks," *IEEE Wireless Commun. Lett.*, vol. 10, no. 11, pp. 2450–2454, Nov. 2021.
[6] D. Song, W. Shin, J. Lee, and H. V. Poor, "Sum-throughput maximization in NOMA-based WPCN: A cluster-specific beamforming approach," *IEEE Internet Things J.*, vol. 8, no. 13, pp. 10543–10556, Jul. 2021.
[7] Q. Shi, L. Liu, W. Xu, and R. Zhang, "Joint transmit beamforming and receive power splitting for MISO SWIPT systems," *IEEE Trans. Wireless Commun.*, vol. 13, no. 6, pp. 3269–3280, Jun. 2014.
[8] Z. Li et al., "Energy efficient resource allocation for UAV-assisted space-air-ground internet of remote things networks," *IEEE Access*, vol. 7, pp. 145348–145362, Oct. 2019.
[9] Q. Wu, Y. Zeng, and R. Zhang, "Joint trajectory and communication design for multi-UAV enabled wireless networks," *IEEE Trans. Wireless Commun.*, vol. 17, no. 3, pp. 2109–2121, Mar. 2018.
[10] J. Wang, C. Jiang, Z. Wei, C. Pan, H. Zhang, and Y. Ren, "Joint UAV hovering altitude and power control for space-air-ground IoT networks," *IEEE Internet Things J.*, vol. 6, no. 2, pp. 1741–1753, Apr. 2019.
[11] C. Yan, L. Fu, J. Zhang, and J. Wang, "A comprehensive survey on UAV communication channel modeling," *IEEE Access*, vol. 7, pp. 107769–107792, Aug. 2019.
[12] J. Wang, C. Jiang, Z. Han, Y. Ren, R. G. Maunder, and L. Hanzo, "Taking drones to the next level: Cooperative distributed unmanned-aerial-vehicular networks for small and mini drones," *IEEE Veh. Technol. Mag.*, vol. 12, no. 3, pp. 73–82, Sep. 2017.
[13] M. Alzenad, A. El-Keyi, F. Lagum, and H. Yanikomeroglu, "3-D placement of an unmanned aerial vehicle base station (UAV-BS) for energy-efficient maximal coverage," *IEEE Wireless Commun. Lett.*, vol. 6, no. 4, pp. 434–437, Aug. 2017.
[14] X. Sun, W. Yang, and Y. Cai, "Secure communication in NOMA-assisted millimeter-wave SWIPT UAV networks," *IEEE Internet Things J.*, vol. 7, no. 3, pp. 1884–1897, Mar. 2020.
[15] W. Wang et al., "Joint precoding optimization for secure SWIPT in UAV-aided NOMA networks," *IEEE Trans. Commun.*, vol. 68, no. 8, pp. 5028–5040, Aug. 2020.
[16] Z. Chen, K. Chi, K. Zheng, G. Dai, and Q. Shao, "Minimization of transmission completion time in UAV-enabled wireless powered communication networks," *IEEE Internet Things J.*, vol. 7, no. 2, pp. 1245–1259, Feb. 2020.
[17] Q. Wu and R. Zhang, "Intelligent reflecting surface enhanced wireless network via joint active and passive beamforming," *IEEE Trans. Wireless Commun.*, vol. 18, no. 11, pp. 5394–5409, Nov. 2019.
[18] Z. Li, W. Chen, Q. Wu, H. Cao, K. Wang, and J. Li, "Robust beamforming design and time allocation for IRS-assisted wireless powered communication networks," *IEEE Trans. Commun.*, vol. 70, no. 4, pp. 2838–2852, Apr. 2022.
[19] Q. Wu and R. Zhang, "Beamforming optimization for wireless network aided by intelligent reflecting surface with discrete phase shifts," *IEEE Trans. Commun.*, vol. 68, no. 3, pp. 1838–1851, Mar. 2020.
[20] Z. Li, W. Chen, and H. Cao, "Beamforming design and power allocation for transmissive RMS-based transmitter architectures," *IEEE Wireless Commun. Lett.*, vol. 11, no. 1, pp. 53–57, Jan. 2022.
[21] K. Wang, Y. Zhou, Q. Wu, W. Chen, and Y. Yang, "Task offloading in hybrid intelligent reflecting surface and massive MIMO relay networks," *IEEE Trans Wireless Commun.*, vol. 21, no. 6, pp. 3648–3663, Jun. 2022.
[22] Z. Li, W. Chen, J. Lu, K. Wang, and J. Li, "Uplink transceiver design and optimization for transmissive RMS multi-antenna systems," 2021, *arXiv:2112.08880*.
[23] S. Gong et al., "Towards smart radio environment for wireless communications via intelligent reflecting surfaces: A comprehensive survey," 2019, *arXiv:1912.07794*.
[24] W. Tang et al., "Wireless communications with reconfigurable intelligent surface: Path loss modeling and experimental measurement," *IEEE Trans. Wireless Commun.*, vol. 20, no. 1, pp. 421–439, Jan. 2021.
[25] M. Hua and Q. Wu, "Joint dynamic passive beamforming and resource allocation for IRS-aided full-duplex WPCN," *IEEE Trans. Wireless Commun.*, vol. 21, no. 7, pp. 4829–4843, Jul. 2022.
[26] Z. Li, W. Chen, Q. Wu, K. Wang, and J. Li, "Joint beamforming design and power splitting optimization in IRS-assisted SWIPT NOMA networks," *IEEE Trans. Wireless Commun.*, vol. 21, no. 3, pp. 2019–2033, Mar. 2022.
[27] T. Shafique, H. Tabassum, and E. Hossain, "Optimization of wireless relaying with flexible UAV-borne reflecting surfaces," *IEEE Trans. Commun.*, vol. 69, no. 1, pp. 309–325, Jan. 2021.
[28] X. Mu, Y. Liu, L. Guo, J. Lin, and H. V. Poor, "Intelligent reflecting surface enhanced multi-UAV NOMA networks," *IEEE J. Sel. Areas Commun*, vol. 39, no. 10, pp. 3051–3066, Oct. 2021.
[29] S. Li, B. Duo, M. D. Renzo, M. Tao, and X. Yuan, "Robust secure UAV communications with the aid of reconfigurable intelligent surfaces," *IEEE Trans. Wireless Commun.*, vol. 20, no. 10, pp. 6402–6417, Oct. 2021.
[30] Z.-Q. He and X. Yuan, "Cascaded channel estimation for large intelligent metasurface assisted massive MIMO," *IEEE Wireless Commun. Lett.*, vol. 9, no. 2, pp. 210–214, Feb. 2020.
[31] G. T. de Araújo, A. L. F. de Almeida, and R. Boyer, "Channel estimation for intelligent reflecting surface assisted MIMO systems: A tensor modeling approach," *IEEE J. Sel. Topics Signal Process.*, vol. 15, no. 3, pp. 789–802, Apr. 2021.
[32] N. Senadhira, S. Durrani, X. Zhou, N. Yang, and M. Ding, "Uplink NOMA for cellular-connected UAV: Impact of UAV trajectories and altitude," *IEEE Trans. Commun.*, vol. 68, no. 8, pp. 5242–5258, Aug. 2020.
[33] C. You and R. Zhang, "3D trajectory optimization in Rician fading for UAV-enabled data harvesting," *IEEE Trans. Wireless Commun.*, vol. 18, no. 6, pp. 3192–3207, Jun. 2019.
[34] Y. Liu, Z. Qin, M. Elkashlan, Z. Ding, A. Nallanathan, and L. Hanzo, "Nonorthogonal multiple access for 5G and beyond," *Proc. IEEE*, vol. 105, no. 12, pp. 2347–2381, Dec. 2017.
[35] K. Xiong, B. Wang, and K. J. R. Liu, "Rate-energy region of SWIPT for MIMO broadcasting under nonlinear energy harvesting model," *IEEE Trans. Wireless Commun.*, vol. 16, no. 8, pp. 5147–5161, Aug. 2017.
[36] M. Hua, L. Yang, Q. Wu, and A. L. Swindlehurst, "3D UAV trajectory and communication design for simultaneous uplink and downlink transmission," *IEEE Trans. Commun.*, vol. 68, no. 9, pp. 5908–5923, Sep. 2020.
[37] M. Grant and S. Boyd, "CVX: Matlab software for disciplined convex programming, version 2.1," Mar. 2014. [Online]. Available: http://cvxr.com/cvx
[38] S. Hua, Y. Zhou, K. Yang, Y. Shi, and K. Wang, "Reconfigurable intelligent surface for green edge inference," *IEEE Trans. Green Commun. Netw.*, vol. 5, no. 2, pp. 964–979, Jun. 2021.
[39] S. Boyd, S. P. Boyd, and L. Vandenberghe, *Convex Optimization*. Cambridge, U.K.: Cambridge Univ. Press, 2004.
[40] Y. Lu, K. Xiong, P. Fan, Z. Ding, Z. Zhong, and K. B. Letaief, "Global energy efficiency in secure MISO SWIPT systems with non-linear power-splitting EH model," *IEEE J. Sel. Areas Commun.*, vol. 37, no. 1, pp. 216–232, Jan. 2019.

Zhendong Li received the B.S. degree in communications engineering from Zhengzhou University, Zhengzhou, China, in 2017, and the master's degree in telecommunication and information systems from the Beijing University of Posts and Telecommunications, Beijing, China, in 2020. He is currently working toward the Ph.D. degree with the Broadband Access Network Laboratory, Department of Electronic Engineering, Shanghai Jiao Tong University, Shanghai, China. His research interests include reconfigurable meta-surface, unmanned aerial vehicle communications, space-air-ground networks, Internet-of-Things, and wireless resource management in future wireless networks.

Wen Chen (Senior Member, IEEE) is currently a tenured Professor with the Department of Electronic Engineering, Shanghai Jiao Tong University, Shanghai, China, where he is also the Director of the Broadband Access Network Laboratory. He has authored or coauthored more than 100 articles in IEEE journals and more than 120 papers in IEEE Conferences, with citations more than 7000 in Google Scholar. His research interests include reconfigurable meta-surface, multiple access, wireless AI, and green networks. He is a Fellow of the Chinese Institute of Electronics and the distinguished Lecturer of IEEE Communications Society and IEEE Vehicular Technology Society. He is the Shanghai Chapter Chair of IEEE Vehicular Technology Society, the Editor of IEEE TRANSACTIONS ON WIRELESS COMMUNICATIONS, IEEE TRANSACTIONS ON COMMUNICATIONS, IEEE ACCESS, and IEEE OPEN JOURNAL OF VEHICULAR TECHNOLOGY.

Huanqing Cao received the B.S. degree in electronic information engineering from Beihang University, Beijing, China, in 2019. He is currently working toward the master's degree with Broadband Access Network Laboratory, Department of Electronic Engineering, Shanghai Jiao Tong University, Shanghai, China. His research interests include reconfigurable meta-surface and wireless resource management in future wireless networks.

Hongying Tang received the Ph.D. degree from Shanghai Jiao Tong University, Shanghai, China, in 2015. She is currently a Senior Engineer with the Science and Technology on Microsystem Laboratory, Shanghai Institute of Microsystem and Information Technology, Chinese Academy of Sciences, Beijing, China. Her research interests include unmanned aerial vehicle communications and MAC protocols in wireless sensor networks.

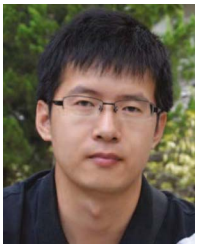

Kunlun Wang (Member, IEEE) received the Ph.D. degree in electronic engineering from Shanghai Jiao Tong University, Shanghai, China, in 2016. From 2016 to 2017, he was with Huawei Technologies Company, Ltd., where he was involved in energy efficiency algorithm design. From 2017 to 2019, he was with the Key Lab of Wireless Sensor Network and Communication, SIMIT, Chinese Academy of Sciences, Shanghai, China. From 2019 to 2020, he was with the School of Information Science and Technology, ShanghaiTech University, Shanghai, China. Since 2021, he has been a Professor with the School of Communication and Electronic Engineering, East China Normal University, Shanghai, China. His current research interests include energy efficient communications, fog computing networks, resource allocation, and optimization algorithm.

Jun Li (Senior Member, IEEE) received the Ph.D. degree in electronic engineering from Shanghai Jiao Tong University, Shanghai, China, in 2009. From January 2009 to June 2009, he was a Research Scientist with the Department of Research and Innovation, Alcatel Lucent Shanghai Bell. From June 2009 to April 2012, he was a Postdoctoral Fellow with the School of Electrical Engineering and Telecommunications, The University of New South Wales, Kensington, NSW, Australia. From April 2012 to June 2015, he was a Research Fellow with the School of Electrical Engineering, The University of Sydney, Sydney, NSW, Australia. Since 2015, he has been a Professor with the School of Electronic and Optical Engineering, Nanjing University of Science and Technology, Nanjing, China. From 2018 to 2019, he was a Visiting Professor with Princeton University, Princeton, NJ, USA. He has coauthored more than 200 papers in IEEE journals and conferences, and holds one U.S. patents and more than ten Chinese patents in his research areas, which include network information theory, game theory, distributed intelligence, multiple agent reinforcement learning, and their applications in ultra-dense wireless networks, mobile edge computing, network privacy and security, and industrial Internet of Things. He is the Editor of IEEE TRANSACTIONS ON WIRELESS COMMUNICATIONS. He was the Editor of IEEE COMMUNICATION LETTERS and TPC Member of several flagship IEEE conferences. He was the recipient of Exemplary Reviewer of IEEE TRANSACTIONS ON COMMUNICATIONS in 2018, and Best Paper Award from IEEE International Conference on 5G for Future Wireless Networks in 2017.